Title: Calmodulin inhibition regulates morphological and functional changes related to the actin cytoskeleton in pure microglial cells

Author: Melinda Szabo Karolina Dulka Karoly Gulya

PII: S0361-9230(15)30057-5
DOI: http://dx.doi.org/doi:10.1016/j.brainresbull.2015.11.003
Reference: BRB 8916

To appear in: *Brain Research Bulletin*

Received date: 8-9-2015
Revised date: 26-10-2015
Accepted date: 3-11-2015

Please cite this article as: Melinda Szabo, Karolina Dulka, Karoly Gulya, Calmodulin inhibition regulates morphological and functional changes related to the actin cytoskeleton in pure microglial cells, Brain Research Bulletin http://dx.doi.org/10.1016/j.brainresbull.2015.11.003

Calmodulin inhibition regulates morphological and functional changes related to the actin cytoskeleton in pure microglial cells

Running title: Calmodulin inhibition in cultured microglia

Melinda Szabo, Karolina Dulka, Karoly Gulya* gulyak@bio.u-szeged.hu

Department of Cell Biology and Molecular Medicine, University of Szeged, Szeged, Hungary

*Corresponding author at: Department of Cell Biology and Molecular Medicine, University of Szeged, 4 Somogyi u., Szeged, H-6720, Hungary. Tel.: 36 (62) 544-570, fax: 36 (62) 544-569.

Highlights

CaM inhibitors were tested in unchallenged and in LPS-challenged pure microglia.

CaM inhibitors affected many morphological and functional aspects of these cells.

CaM, Iba1 intracellular distribution and actin cytoskeleton remodeling were affected.

CaM inhibitors differentially affected cell proliferation and viability.

The inhibitors differentially altered phagocytosis in cells with or without LPS.

Abstract

The roles of calmodulin (CaM), a multifunctional intracellular calcium receptor protein, as concerns selected morphological and functional characteristics of pure microglial cells derived from mixed primary cultures from embryonal forebrains of rats, were investigated through use of the CaM antagonists calmidazolium (CALMID) and trifluoperazine (TFP). The intracellular localization of the CaM protein relative to phalloidin, a bicyclic heptapeptide that binds only to filamentous actin, and the ionized calcium-binding adaptor molecule 1 (Iba1), a microglia-specific actin-binding protein, was determined by immunocytochemistry, with quantitative analysis by immunoblotting. In unchallenged and untreated (control) microglia, high concentrations of CaM protein were found mainly perinuclearly in ameboid microglia, while the cell cortex had a smaller CaM content that diminished progressively deeper into the branches in the ramified microglia. The amounts and intracellular distributions of both Iba1 and CaM proteins were altered after lipopolysaccharide (LPS) challenge in activated microglia. CALMID and TFP exerted different, sometimes opposing, effects on many morphological, cytoskeletal and functional characteristics of the microglial cells. They affected the CaM and Iba1 protein expressions and their intracellular localizations differently, inhibited cell proliferation, viability and fluid-phase phagocytosis to different degrees both in unchallenged and in LPS-treated (immunologically challenged) cells, and differentially affected the reorganization of the actin cytoskeleton in the microglial cell cortex, influencing lamellipodia, filipodia and podosome formation. In summary, these CaM antagonists altered different aspects of filamentous actin-based cell morphology and related functions with variable efficacy, which could be important in deciphering the roles of CaM in regulating microglial functions in health and disease.

Abbreviations

Ca^{2+}: calcium ion

CALMID: calmidazolium; 1-[bis(4-chlorophenyl)methyl]-3-[2-(2,4-dichlorophenyl)-2-(2,4-dichlorobenzyloxy)ethyl]-1H-imidazolium chloride

CaM: calmodulin

CNS: central nervous system

DIV: days in vitro

DMEM: Dulbecco's Modified Eagle's Medium

GAPDH: glyceraldehyde 3-phosphate dehydrogenase (EC 1.2.1.12)

Iba1: ionized calcium binding adaptor molecule 1

Ki67: proliferation marker antigen identified by the monoclonal antibody Ki67

LPS: bacterial lipopolysaccharide

mRNA: messenger ribonucleic acid

PBS: phosphate-buffered saline

RT: room temperature

S.E.M.: standard error of mean

subDIV: subcloned days in vitro

TBS: Tris-buffered saline

TFP: trifluoperazine; 10-[3-(4-methylpiperazin-1-yl)propyl]-2-trifluoromethyl-10H-phenothiazine dihydrochloride

TI: transformation index

Keywords: calmidazolium; cell viability; ionized calcium-binding adaptor molecule 1; lipopolysaccharide; phagocytosis; phalloidin; proliferation; trifluoperazine

1. Introduction

Microglia originate from bone marrow-derived myeloid precursors as a unique class of the monocyte/macrophage lineage that infiltrates the central nervous system (CNS) during its early development (Ginhoux et al., 2010; Saijo and Glass, 2011). They respond rapidly to inflammatory cues and injury by transforming from a ramified, resting state to an activated, phagocytic ameboid cell type (Kreutzberg, 1996). In their non-activated or resting state, they display a ramified morphology and subdued macrophage-like functional properties. In response to injury, infection, inflammatory or other signals, the microglia become activated and a series of morphological, molecular and functional changes take place that affect proliferation, homing and adhesion to damaged cells, phagocytosis, antigen presentation and cytotoxic and inflammation-mediating signaling (Drew and Chavis, 2000; Prinz and Miller, 2014; Saijo and Glass, 2011; Streit at al., 1999; Town et al., 2005).

Microglial functions such as motility and phagocytosis are closely associated with dynamic changes in the cytoskeleton and related to intracellular calcium (Ca^{2+}) signaling (Greenberg, 1995; Kalla et al., 2003; Mitchison and Cramer, 1996). The ubiquitous Ca^{2+}-binding proteins participate in Ca^{2+}-elicited intracellular events, either as Ca^{2+}-sensing/receptor/trigger or as Ca^{2+}-buffering/transport proteins, by binding intracellularly stored Ca^{2+} (Ikura, 1996). They contribute to nearly all aspects of the functioning of the cell, and are important in numerous intracellular signaling processes, from the regulation of cellular homeostasis to learning and memory (Berridge et al., 2010; Clapham, 2007). Calmodulin (CaM), one of the most important intracellular Ca^{2+} receptors, exerts its biological action through its heterogenous population of target proteins, which are involved in a number of cellular regulatory processes (Kennedy, 1989; Palfi et al., 2002).

The nervous tissue is especially abundant in CaM. While its distribution has been characterized in detail for a number of neuronal cell types (Kovacs and Gulya, 2002, 2003; Palfi et al., 1999, 2001, 2005), its localization and functions in glial cells are much less known. Astrocytes express CaM protein in low quantities (Kortvely et al., 2003), but mRNA populations from all three CaM genes could still be localized both perinuclearly and in the astrocytic endfeet (Palfi et al., 2005). The expression of CaM in oligodendroglia is similarly low and has not been characterized extensively,

albeit the regulatory effects of this protein on a number of membrane-bound target proteins such as the myelin basic protein (Libich and Harauz, 2008) or the 2',3'-cyclic nucleotide 3'-phosphodiesterase (Myllykoski et al., 2012) have been established. Of all the glial components, only the microglia seem to have a considerable amount of CaM. They express a relatively large amount of CaM when activated (Casal ez al., 2001; Solá et al., 1997), and many aspects of their Ca^{2+} signaling are well documented (Färber and Kettelmann, 2006; Wong and Schlichter, 2014).

CaM immunoreactivity or CaM gene-specific transcripts are often colocalized with those of the target enzymes of CaM within the same cytoplasmic compartments (Erondu and Kennedy, 1985; Sanabria et al., 2008; Seto-Ohshima et al., 1983; Strack et al., 1996). For example, actin is accompanied by CaM in the cell cortex, helping to remodel the actin-based cytoskeleton in accordance with the actual (patho)physiological signals (Mitchison and Cramer, 1996; Psatha et al., 2004). Ionized calcium-binding adaptor molecule 1 (Iba1) is another intracellular Ca^{2+}-binding protein with actin-binding capability that is expressed in macrophages and microglia, and is widely used to detect both resting and activated microglial phenotypes (Imai et al., 1996). CaM and Iba1 proteins share a number of molecular structural variants that are related to either their Ca^{2+} binding or their target protein recognition (Yamada et al., 2006). In contrast with the wide-ranging regulatory roles of CaM, Iba1 plays a much more restricted role in microglial functions, e.g. remodeling the actin cytoskeleton during migration (Siddiqui et al., 2012; Vincent et al., 2012).

The modulatory action of Ca^{2+}-bound CaM on multiple target proteins can be regulated by a number of compounds. Calmidazolium (CALMID; 1-[bis(4-chlorophenyl)methyl]-3-[2-(2,4-dichlorophenyl)-2-(2,4-dichlorobenzyloxy)ethyl]-1H-imidazolium chloride) and trifluoperazine (TFP; 10-[3-(4-methylpiperazin-1-yl)propyl]-2-trifluoromethyl-10H-phenothiazine dihydrochloride) are potent inhibitors of CaM-related cellular activities (Borsa et al., 1986; Sunagawa et al., 2000). It is presumed that, apart from binding to the CaM protein (Mashushima et al., 2000; Vandonselaar et al., 1994; Vertessy et al., 1998), they can also exert their effects on some of the CaM-regulated targets directly (Sunagawa et al., 2000).

In contrast with the extensive studies on the involvement of CaM in a number of neuronal phenomena, only limited information is available on its role in the development and maintenance of the microglial phenotype and its specific functions. Relatively little is known, for example, as concerns the possible involvement of CaM mediation in such important microglial functions as phagocytosis and the cellular functions associated with it, e.g. dynamic cytoskeletal reorganization. Thus, in view of the importance of CaM-mediated cell functions and the paucity of data on specific microglial functions related to and possibly regulated by CaM, we set out to investigate the localization and intracellular distribution of CaM in pure microglial cell populations derived from rat primary mixed forebrain cultures by using immunocytochemical and Western blot techniques. Selected CaM inhibitors such as CALMID and TFP, previously reported to have different modes of action (Matsushima et al., 2000; Sunagawa et al., 2000), were quantitatively tested for their ability to modify the microglial morphology, lamellipodia, filipodia and podosome formation, and specific functions such as cell proliferation and survival, protein expression and phagocytosis in unchallenged (control) and lipopolysaccharide (LPS)-challenged cells. Stimulation with LPS was used to evaluate the ability of microglial cells to respond to activation (Fricker et al., 2012; Song et al., 2014; Tokes et al., 2011).

2. Material and methods

All animal experiments were carried out in strict compliance with the European Council Directive (86/609/EEC) and EC regulations (O.J. of EC No. L 358/1, 18/12/1986) regarding the care and use of laboratory animals for experimental procedures, and followed the relevant Hungarian and local legislation requirements. The experimental protocols were approved by the Institutional Animal Welfare Committee of the University of Szeged (I-74-11/2009/MÁB). The pregnant Sprague-Dawley rats (180-200 g) were kept under standard housing conditions and fed ad libitum.

2.1. Antibodies

The antibodies used in the immunocytochemical and Western blot studies are listed in Table 1. For a thorough characterization of different microglial phenotypes developed in vitro, an antibody against Iba1, an intracellular actin- and Ca^{2+}-binding protein expressed in the CNS specifically in macrophages and microglia (Imai et al., 1996; Ahmed et al., 2007), was used in our immunocytochemical and Western blot analyses. An anti-CaM monoclonal antibody was used to detect both Ca^{2+}-bound and Ca^{2+}-free forms of the antigen (Sacks et al., 1991). The anti-Ki67 antibody was used to detect proliferating cells. Ki67 is a nuclear protein expressed in all active phases of the cell cycle from the late G1 phase through the end of the M phase but is absent in non-proliferating and early G1 phase cells (Scott et al., 2004). The anti-glyceraldehyde 3-phosphate dehydrogenase (GAPDH) antibody was used as an internal control in Western blot experiments (Wu et al., 2012). Dilutions of primary and secondary antibodies, and also incubation times and blocking conditions for each antibody used were carefully tested for both immunocytochemistry and Western blot analysis. To detect the specificities of the secondary antisera, omission control experiments (staining without the primary antibody) were performed. In such cases, no fluorescent or Western blot signals were detected.

2.2. Preparation of primary mixed cortical cell cultures

Mixed primary cortical cell cultures were established from embryonic day 18 (E18) wild-type rat embryos by the use of the methods described previously (Szabo and Gulya, 2013). Briefly, 6-8 fetal rats under deep ether anesthesia were surgically decapitated and the frontal lobe of the cerebral cortex was removed, minced with scissors, and incubated in 9 ml Dulbecco's Modified Eagle's Medium (DMEM; Invitrogen, Carlsbad, CA, USA) containing 1 g/l D-glucose, 110 mg/l Na-pyruvate, 4 mM L-glutamine, 3.7 g/l $NaHCO_3$, 10,000 U/ml penicillin G, 10 mg/ml streptomycin sulfate and 25 μg/ml amphotericin B) and supplemented with 0.25% trypsin (Invitrogen) for 10 min at 37 °C, then centrifuged at 1,000*g* for 10 min at room temperature (RT). The pellet was resuspended and washed twice in 5 ml DMEM containing 10% heat-inactivated fetal bovine serum (FBS; Invitrogen) and centrifuged for 10 min at 1,000*g* at RT. The final pellet was resuspended in 2 ml of

the same solution as above, after which the cells were seeded in the same medium and cultured at 37 °C in a humidified air atmosphere supplemented with 5% CO_2 in one or other of the following ways: 1) in poly-L-lysine-coated coverslips (18 x 18 mm; 2 x 10^5 cells/coverslip) for immunocytochemistry; 2) in poly-L-lysine-coated Petri dishes (60 mm x 15 mm; 10^6 cells/dish) for Western blot analyses; or 3) in a poly-L-lysine-coated culture flask (75 cm^2 , 12 x 10^6 cells/flask) for the subsequent generation of pure microglial cell cultures. The mixed primary cultures were maintained up to 28 days (DIV1-DIV28) for immunocytochemistry and Western blot analyses, and for 7 days (DIV7) for the generation of pure microglial cells. For culturing periods longer than 3 days, the DMEM was changed every 3 days.

2.3. Preparation of pure microglial cell cultures

Pure microglial cell cultures were subcloned from mixed primary cultures (DIV7) maintained in a poly-L-lysine-coated culture flask (75 cm^2 , 12 x 10^6 cells/flask) by shaking the cultures at 150 rpm in a platform shaker for 20 min at 37 °C. Microglia from the supernatant were collected by centrifugation at 3,000*g* for 10 min at RT and resuspended in 2 ml of DMEM/10% FBS. The cells were seeded at a density of 2 x 10^5 cells/Petri dish for Western blots and cell viability assays or 10^5 cells/coverslip/Petri dish for immunocytochemistry, proliferation or phagocytosis assays, and cultured in DMEM in a humidified atmosphere supplemented with 5% CO_2 for 4 days at 37 °C. The medium was changed on the first day after seeding (subDIV1). Immunocytochemistry routinely performed on the pure microglial cultures 4 days after seeding (subDIV4) consistently detected a >99% incidence of Iba1-immunopositive microglial cells for the Hoechst 33258 dye-labeled cell nuclei (Figure 2).

2.4. Treatment of pure microglial cells with LPS and CaM inhibitors

On the fourth day of subcloning (subDIV4), the DMEM was replaced and the expanded pure microglial cells were treated for 24 h with either LPS (100 ng/ml in final concentration, dissolved in DMEM; Sigma, St. Louis, MO, USA), CALMID (5 nM or 50 nM in final concentration, dissolved in dimethylsulfoxide (DMSO); Sigma) or TFP (10 μM or 20 μM final concentration, dissolved in DMSO; Sigma) alone, or with

a combination of LPS and one of these CaM inhibitors, and the effects were compared in a variety of morphological and functional tests. LPS treatment served as an immunochallenge. Unchallenged and untreated (control) cultures were maintained under identical conditions, but without these inhibitors, and received 2 μl DMSO solution instead.

2.5. Immunocytochemistry

For immunocytochemistry, primary cortical cells (DIV1-DIV28) or pure microglial cells (subDIV4) cultured in vitro on poly-L-lysine-coated coverslips were used. At different time intervals (DIV1, DIV4, DIV7, DIV10, DIV14, DIV21, DIV28), or after different treatments (subDIV4), the cultured cells on the coverslips were fixed in 4% formaldehyde in 0.05 M phosphate-buffered saline (PBS; pH 7.4 at RT) for 5 min and rinsed in 0.05 M PBS for 3 x 5 min. After permeabilization and blocking of the nonspecific sites in 0.05 M PBS solution containing 5% normal goat serum (Sigma), 1% heat-inactivated bovine serum albumin (Sigma) and 0.05% Triton X-100 for 30 min at 37 °C, the cells on the coverslips were incubated with the appropriate primary antibody (Table 1) in the above solution overnight at 4 °C. The cultured cells were washed for 4 x 10 min at RT in 0.05 M PBS, then incubated with the appropriate Alexa Fluor fluorochrome-conjugated secondary antibody (Table 1) in the above solution, but without Triton X-100, in the dark for 3 h at RT. The cells on the coverslip were washed for 4 x 10 min in 0.05 M PBS at RT. At this stage, the cells were occasionally stained with rhodamine-phalloidin (5 μl in 200 μl PBS; Molecular Probes, Eugene, OR, USA) for 30 min at RT, then washed for 2 x 10 min at RT. Finally, the cell nuclei were stained in a 0.05 M PBS solution containing 1 mg/ml polyvinylpyrrollidone and 0.5 μl/ml Hoechst 33258 dye (Sigma). The coverslips were rinsed in distilled water for 5 min, air-dried and mounted on microscope slides in Vectashield mounting medium (Vector Laboratories, Burlingame, CA, USA). Cells were viewed on a Nikon Microphot-FXA epifluorescent microscope (Nikon Corp., Tokyo, Japan) and photographed with a Spot RT Color CCD camera (SPOT RT/ke, Diagnostic Instruments, Inc., Sterling Heights, MI, USA).

2.6. Western blot analysis

For Western blots, the protocols were optimized for each antibody as regards epitope accessibility, polyacrylamide gel separation, antibody dilution and chemiluminescence signal intensity. Cultured primary cells (DIV1–DIV28) or pure microglial cells (subDIV4) with different treatment regimens were collected through use of a rubber policeman, homogenized in 50 mM Tris-HCl (pH 7.5) containing 150 mM NaCl, 0.1% Nonidet P40, 0.1% cholic acid, 2 μg/ml leupeptin, 1 μg/ml pepstatin, 2 mM phenylmethylsulfonyl fluoride and 2 mM EDTA, and centrifuged at 10,000*g* for 10 min at 4 °C. The pellet was discarded and the protein concentration of the supernatant was determined (Lowry et al., 1951). For the Western blot analyses of Iba1, CaM and GAPDH immunoreactivities, 5-10 μg of heat-denatured protein was separated on an SDS polyacrylamide gel. The stacking gel/resolving gel ratio was 4-10% for Iba1 and GAPDH, and 4-16% for CaM immunoreactivities; for CaM Westerns, the stacking gel was complemented with 16% urea and 16% glycerol. Separated proteins were then transferred onto Hybond-ECL nitrocellulose membrane (Amersham Biosciences, Little Chalfont, Buckinghamshire, England). Strips of membranes with the transferred bands for CaM and Iba1 (both around 17 kDa) and GAPDH (37 kDa) were cut and processed separately for CaM, Iba1 or GAPDH immunodetection. The membranes were blocked for 1 h in 5% nonfat dry milk (for Iba1 and GAPDH Westerns) or 5% bovine serum albumin (for CaM Westerns) in Tris-buffered saline (TBS) containing 0.1% Tween 20, and incubated for 1 h with the appropriate primary antibodies (Table 1). After 5 washes in 0.1% TBS–Tween 20, the membranes were incubated for 1 h with the appropriate peroxidase-conjugated secondary antibodies (Table 1), and washed 5 times as before. The enhanced chemiluminescence method (ECL Plus Western blotting detection reagents; Amersham Biosciences) was used to reveal immunoreactive bands according to the manufacturer's protocol. The immunoreactive densities of equally loaded lanes were quantified, and all samples were normalized to internal GAPDH load controls run on the same gels.

2.7. Cell proliferation and cell viability assays

For the assessment of CaM inhibition on cell proliferation and survival, pure microglial cells (subDIV4) were cultured in DMEM with or without the appropriate test compounds in a humidified atmosphere supplemented with 5% CO_2 at 37 °C for 24 h. To analyze the effects of these treatments on cell proliferation, the cultures were processed for Ki67 immunocytochemistry. Proliferation index (PI) was defined as the number of Ki67-positive microglial cell nuclei per 1,000 analyzed Iba1-positive cells and usually expressed as % of the total cells analyzed (Brownhill et al., 2014; Yamaguchi et al., 2013). A total of 1,454 fields of view with 55,565 Iba1-positive and 783 Ki67-positive/Iba1-positive microglia were analyzed across the groups (mean ± S.E.M.).

To estimate the surviving microglial cells after treatments, the cultures were washed twice with 2 ml of PBS to remove cell debris and treated with 0.25% trypsin solution for 10 min at 37 °C, collected and counted in a Burker cell. The number of viable cells was presented as mean ± S.E.M.

2.8. In vitro phagocytosis assay

The fluid-phase phagocytic capacity of the microglial cells was determined via the uptake of fluorescent microspheres (2 μm in diameter; Sigma) using the general methods described by Szabo and Gulya (2013). Unstimulated (control) and LPS-stimulated pure microglial cell cultures with or without CaM inhibition were tested for 24 h. At the end of the culturing period (subDIV4), 1 μl of a 2.5% aqueous suspension of fluorescent microspheres was added per ml of the culture, which was then further incubated for 60 min at 37 °C. The cells were next washed 5 times with 2 ml of PBS to remove dish- or cell surface-bound residual fluorescent microspheres, and fixed with 4% formalin in PBS. For measurement of the phagocytic activity, Iba1-expressing microglia labeled with phagocytosed microbeads were counted. Negative controls were treated as above with the exception that microglial cultures with beads were incubated for 60 min at 4 °C. At this temperature, the number of beads associated with cell surface averaged less than 1 bead per 100 Iba1-labeled cells. For the study of the effects of CaM inhibitors on the number of phagocytosed beads (mean ± S.E.M.), a total of 873 bead-labeled

cells were counted in three separate culturing procedures under a Nikon Microphot-FXA epifluorescent microscope with a 10x or 20x objective.

2.9. Digital image processing and image analysis

Gray scale digital images of the Western blots were acquired by scanning the autoradiographic films with a desktop scanner (Epson Perfection V750 PRO; Seiko Epson Corp., Japan). The images were scanned and processed at identical settings to allow comparisons of the Western blots from different samples. Digital images were acquired with a Nikon Microphot-FXA epifluorescent microscope (Nikon Corp., Tokyo, Japan), using a Spot RT Color CCD camera and Spot RT software (Spot RT/ke Diagnostic Instruments). Microglial cell silhouettes were acquired by transforming the raw digital files of Iba1-immunoreactive cells made under fluorescent microscope light to binary files, using the ImageJ software (version 1.47; developed at the U.S. National Institutes of Health by W. Rasband, and available from the Internet at http://rsb.info.nih.gov/ij). The color cell images were transformed into their binary replicas (silhouettes) through automatic thresholding procedures (Szabo and Gulya, 2013). After thresholding, values for cell perimeter (μm) and cell area (μm^2) were determined from at least 3 separate experiments (at least 2 coverslips in each experiment for each culturing time investigated; about 20 randomly selected cells/coverslip), and the transformation index (TI) reflecting the degree of process extension was calculated via an expression [perimeter of cell (μm)]^2/4π[cell area (μm^2)] as previously described (Fujita et al., 1996). For the analysis of TI values, a total of 261 cells were quantitatively measured (mean ± S.E.M.). Digital image production was performed with Adobe Photoshop CS5.1 software (Adobe Systems, Inc., San Jose, CA, USA). Color correction (brightness, contrast) and cropping of the fluorescent images were occasionally performed when individual photomicrographs were assembled to figure panels for publication. No specific feature within an image was enhanced, obscured, introduced, moved or removed.

2.10. Statistical analysis

All statistical comparisons were made with SigmaPlot (v. 12.3, Systat Software Inc., Chicago, IL, USA). Results for the phagocytosis and viability assays and the cell silhouette characteristics (TI values) were analyzed with Kruskal-Wallis one-way analysis of variance, followed by Dunn's method for pairwise multiple comparison procedures for statistically significant differences between the groups. For these studies, values were presented as mean ± S.E.M. from at least three independent experiments and $p<0.05$ was considered significant. For Western blots, values were presented as mean ± S.E.M. from at least three blots, each representing independent experiments for each time period examined. For the determination of the homogeneity of the subcloned microglial cells, Iba1-positive cells and Hoechst 33258 dye-positive cell nuclei from at least 50 randomly sampled microscope fields from 2-3 coverslips for each subcloned culture were counted and the results are presented as mean ± S.E.M.

3. Results

3.1. CaM is differentially localized in ameboid and ramified microglia both in mixed and pure cultures

The quantity and cell type-specific localization of the CaM protein was first established in mixed primary cultures under unstimulated and untreated (control) conditions. Fluorescent immunocytochemistry (Figure 1A-P) and Western blot analysis (Figure 1Q, R) demonstrated that a high concentration of CaM protein was characteristic of the mixed cultures throughout culturing. In young cultures (DIV1-DIV7), when only a few cells double-positive for the Iba1 (Figure 1A, E) and CaM (Figure 1B, F) antigens existed (Figure 1A-H), most of the CaM immunoreactivity was associated with non-microglial, e.g. mainly neuronal, cell forms, as demonstrated earlier (Szabo and Gulya, 2013). From DIV14 (up to DIV28), as more Iba1-positive microglia populated the cultures (Figure 1I, M), the proportion of CaM immunoreactivity associated with the microglia (Figure 1J, N) also grew steadily. Both ameboid (Figure 1A, E) and ramified microglia (a few cells in Figure 1I, M) expressed CaM immunoreactivity. As the cultures aged, the CaM immunoreactivity

localized to microglia became predominant (compare Figure 1I, M with Figure 1K, O). Similarly, Western blot studies confirmed the increase in Iba1 immunoreactivity during culturing (Figure 1Q), during which time the CaM content of the cultures remained unchanged (Figure 1R). Thus, by DIV14, the microglia had become the main CaM-expressing cell type in the mixed primary forebrain culture.

Subsequent experiments were performed on pure microglial cultures (subDIV4; Figure 2). In these microglial cells the Iba1 immunoreactivity was most intense in the lamellipodia of the ameboid forms (Figure 3A, D, G), followed by the perinuclear region (Figure 3D, G). The strongest CaM immunoreactivity was always observed in the ameboid microglia, where the cell somata, and especially the perinuclear area, were the most intensely labeled (Figure 3B, E, H). In ameboid microglia, the CaM and Iba1 immunoreactivities were distributed in a complementary manner, as the Iba1 protein tending to localize in the cell cortex and lamellipodia (Figure 3A, B, C). The ramified microglia displayed an almost homogenous cytoplasmic Iba1 distribution (Figure 3J) with a considerably lower CaM content typically localized around the nucleus; the branches had only traces of CaM immunoreactivity (Figure 3K, L).

3.2. CALMID and TFP differentially affect microglial proliferation and cell survival

When CaM inhibitors were tested on cell proliferation and cell viability, CALMID and TFP, either alone or in combination with LPS, had different effects (Figure 4A, B). Proliferation was measured as a function of Ki67-immunopositivity of the microglial cells (PI). Unstimulated (control) microglia (subDIV4) had an average PI value of 2.5% (25.22 ± 8.9 Ki67-positive microglia/1,000 analyzed microglia in the culture; Figure 4A). LPS challenge inhibited cell proliferation, albeit without reaching significance (PI = 0.41; 16.2% of the control value). According to Ki67 immunocytochemistry, TFP10 significantly decreased microglial cell proliferation both in unchallenged and LPS-challenged microglia with PI values of 0.21% and 0.12%, respectively (Figure 4A). While CALMID50 treatment alone had no effect on the proliferation of unchallenged microglia, LPS-challenged cells treated with CALMID50 showed some but not significant inhibition.

Cell viability was also investigated in pure microglial cultures (Figure 4B). In contrast with the ineffectivity of CALMID50 on cell survival in unchallenged and in LPS-challenged microglial populations, TFP10 was highly effective in these cultures. In unchallenged cells, TFP10 significantly decreased cell viability to 62.47% of the control value. Similarly, when the microglial cells were challenged by LPS treatment (100 ng/ml), TFP10 effectively decreased the number of surviving cells to 71.28% of the control (Figure 4B).

3.3. CaM inhibition affects cell morphology and actin cytoskeleton reorganization

The microglial morphology in the control and experimental groups was analyzed through binary silhouettes (Figure 5). The quantitative analysis was based on the area, perimeter and TI, the latter being a dimensionless number that is an indicator for the degree of process extension of a cell. Throughout the experiments, microglial cells with TI < 3 were considered ameboid. The unchallenged, untreated 4-day-old pure microglia culture (subDIV4) consisted mainly of ameboid cells (Figure 5, control row; see also controls in Figures 7, 8, 10) with an average area of 412.91 ± 27.2 μm^2, perimeter of 100.73 ± 5.4 μm and a TI of 2.02 ± 0.1 (Figure 6). When administered alone, CALMID and TFP affected TI and the microglial cell surface area and perimeter differently. For example, both CALMID5 and CALMID50 resulted in increased area, perimeter and TI, whereas TFP alone strongly inhibited these characteristics. When challenged with LPS, the microglia became enlarged and acquired significantly larger perimeter and TI (A = 777.23 ± 40.1 μm^2, P = 238.97 ± 8.6 μm, TI = 6.14 ± 0.4), consistent with these cells becoming activated (Figures 5, 6 and Figure 7D-F). Interestingly, CALMID5 or CALMID50 alone was not effective but when used in combination with LPS, they significantly increased the cell surface area, perimeter and TI (Figure 5, Figure 6A, C, E, Figure 7G-I). TFP sigificantly inhibited the expansion of cell surface area and perimeter both in unchallenged and LPS-challenged cells (Figure 6B, D). As an example, the cell surface area was decreased substantially after TFP or LPS+TFP treatment, to 46.4 or 44.5% of the unchallenged or LPS-challenged control value, respectively. TFP treatment was also very effective in decreasing TI, to 25.53% of the LPS-challenged value (Figures 5, 6).

CaM inhibition affected the microglial morphology through reorganization of the actin cytoskeleton (Figure 7). In unchallenged and untreated (control) cultures, the Iba1- and phalloidin-related fluorescence signals largely overlapped in the cell cortex of the mainly ameboid microglia, often in lamellipodia (Figure 7A-C) as expected, since they both bind to the actin cytoskeleton. When treated with LPS, the microglia that became activated and enlarged displayed a phalloidin distribution much fuzzier than that in the case of Iba1, probably due to the rapid association of fibrous actin, to which phalloidin preferentially binds (Figure 7D-F). However, spot-like concentrations of phalloidin fluorescence resembling podosomes were often visible in LPS-treated cells (Figure 7E, arrow). CaM inhibitors affected the Iba1 and phalloidin distributions in different ways. CALMID50 treatment resulted in phalloidin fluorescence that was clearly distributed in two distinct concentric rings in the cytoplasm, one ring in the cell cortex, and the other as a perinuclearly localized cytoplasmic streaming of freshly synthesized fibrous actin (Figure 7H, K, arrows). Phalloidin-containing filipodia were also obvious in these cells. Similar, albeit less dense, Iba1 distribution was observed after CALMID50 treatments (Figure 7G). TFP treatment resulted in an overlapping and almost homogenous distribution of both Iba1 immunoreactivity and phalloidin fluorescence (Figure 7M-O) in the surviving cells. While the Iba1 immunoreactivity remained relatively intact (Figure 7M), most of the phalloidin fluorescence intensity was lost in TFP-treated microglia (Figure 7N) indicating that TFP affected actin polymerization.

3.4. CaM inhibitors differentially alter the intracellular localization of CaM, and affect the Iba1 and CaM protein expressions

CaM inhibitors altered the intracellular localization of CaM protein (Figure 8). Both unchallenged and untreated cells (Figure 8A-C) and LPS-challenged cells (Figure 8D-F) displayed high CaM content primarily localized in the perinuclear compartment and to a much lesser extent with that in the cell cortex (Figure 8A, B). Some of the cells with larger TI had CaM immunoreactivity that progressively diminished toward the cell cortex (Figure 8C). Interestingly, cells treated with CALMID50 alone displayed a more heterogenously translocated CaM immunoreactivity often cortically localized in lamellipodia (Figure 8J-L, arrowheads). In TFP10-treated cells,

the CaM immunoreactivity was very weak and homogenously distributed in the cytoplasm (Figure 8M-O).

CaM antagonists inhibited Iba1 and CaM protein expressions with different efficacies (Figure 9). In general, CALMID was less potent than TFP in affecting Iba1 and CAM protein expressions. CALMID, either alone or in combination with LPS, was not able to alter the Iba1 expression significantly (Figure 9A). TFP was more potent as TFP10 and TFP20 inhibited Iba1 protein expression in a dose-dependent manner both in unchallenged and LPS-challenged cells (Figure 9C). Similarly to their effects on the Iba1 expression, CALMID and TFP antagonized the CaM protein expression with different efficacy (Figure 9B, D). When CALMID was used, the CaM immunoreactivity was observed to decrease somewhat dose-dependently in the unchallenged microglia as CALMID50 significantly inhibited the CaM protein expression to 38.6% of the control level (Figure 9B). Again, TFP20 had a more profound effect on the CaM protein expression (Figure 9D), as it exhibited a strong inhibition both in the unchallenged and in the LPS-activated microglia (20.8% and 23.4% of the control value, respectively).

3.5. CaM inhibition impairs phagocytosis in activated microglia

Cultured microglia readily phagocytosed fluorescently labeled beads (Figure 10, 11). On average, unchallenged and untreated microglia had 3.13 ± 0.1 phagocytosed microbeads per cell (Figure 10A-C and Figure 11). LPS-challenged microglia displayed a large (about 2.8-fold) increase in phagocytotic activity (8.78 ± 0.3; Figure 10D-F and Figure 11). CaM inhibitors affected phagocytosis similarly but with different degrees of potency. CALMID dose-dependently inhibited phagocytosis both in unchallenged and LPS-challenged microglia (Figure 10G-I and Figure 11A). TFP proved to be a very strong inhibitor of phagocytosis both in unchallenged and LPS-challenged microglia (Figure 10M-O and Figure 11B) as it reduced the number of phagocytosed microbeads by almost 90% (to 0.33 ± 0.2; 10.6% of the control value) in unchallenged, and by 76.5% (to 0.75 ± 0.3; 23.5% of the control value) in LPS-challenged cells.

4. Discussion

One of the most ubiquitous Ca^{2+}-sensing proteins is CaM. Its distributions in the developing and the adult rodent brain have been well documented (Caceres et al., 1983; Seto-Ohshima et al., 1983). It is encoded by three different genes in mammals (Palfi et al., 2002; Toutenhoofd and Strehler, 2000). The expression patterns corresponding to the three CaM genes display a broad differential distribution in the developing (Kortvely et al., 2002) and the adult rat CNS under both physiological (Kovacs and Gulya, 2002, 2003; Palfi et al., 1999; Solá et al., 1996) and pathophysiological conditions (Palfi et al., 2001; Palfi and Gulya, 1999; Vizi et al., 2000). Quantitative analysis of the expression patterns of these genes indicated a differential dendritic targeting of the CaM mRNAs (Kortvely et al., 2003; Palfi et al., 1999, 2005); differential intracellular targeting of selected CaM mRNA populations could serve for the local translation of the necessary CaM proteins that regulate the numerous target proteins in that particular cytoplasmic compartment (Kortvely and Gulya, 2004).

CaM expression could be regulated by a number of different physiological and pathophysiological cues. Although its gene expression is generally very stable (Kortvely and Gulya, 2004; Palfi et al., 2002), we have identified many factors that could differentially affect the expressions of the individual CaM genes in neurons with distinct phenotypes from different brain regions (Orojan et al., 2006; Palfi et al., 1999, 2002; Bakota et al., 2005), e.g. inflammation (Orojan et al., 2008), ischemia (Palfi et al., 2001), dehydration (Palfi and Gulya, 1999), and chronic ethanol treatment and withdrawal (Vizi et al., 2000). Apart from the neurons, the microglia display a considerable amount of CaM. This CaM expression, however, is strongly dependent on the phenotype. After a kainic acid challenge, CaM immunoreactivity was earlier demonstrated in reactive microglia of the hippocampus (Solá et al., 1997), where the thickened and shortened microglial processes accumulated CaM protein.

In our studies, CaM was localized both in developing microglial cells of primary cortical cultures established from E18 wild-type rat embryos maintained for up to 28 days (DIV1-28) and in pure microglial cells subcultured from DIV7 cultures for 4 days (subDIV4). Moreover, the presence of CaM protein was

demonstrated not only in reactive microglia (treated with LPS alone or in combination with one of the CaM inhibitors), but also, at a lower protein level, in unchallenged proliferating ameboid or even ramified, microglial cells. We observed morphologically and functionally different microglial populations within the range from weak to strong levels of CaM expression during culturing, as evidenced by their quantitative assessment by fluorescent immunocytochemical and Western blotting methods. In mixed primary cortical cultures, ameboid microglia, the predominant form in the early stages but always present (in much smaller numbers) during culturing (Szabo and Gulya, 2013), expressed strong CaM immunoreactivity throughout the cytoplasm, while ramified microglia, the typical form in the later stages of microglial development, showed a weaker and more evenly distributed CaM immunoreactivity. A similar intracellular distribution of CaM protein expression was observed in pure microglial cultures. In unchallenged and LPS-challenged cultures, most of the microglia was ameboid and had strong CaM immunoreactivity throughout the cytoplasm. Treatments with CaM inhibitors, both in unchallenged and LPS challenged cells, resulted in a weaker and more homogenously localized CaM immunoreactivity.

We found that the intracellular localization of CaM immunoreactivity described above was closely related, and typically complementary, to the filamentous actin cytoskeleton, comprised mainly of branched F-actin (Rotty et al., 2013). F-actin was visualized in our studies by the distributions of an actin-binding protein, Iba1, and phalloidin, a bicyclic heptapeptide that recognizes F-actin only, e.g. the form that possesses cellular functionality. Iba1 is an intracellular Ca^{2+}-binding protein that plays an important role in regulation of the intracellular actin dynamics through the direct binding of actin, enhances membrane ruffling and participates in phagocytosis and cell motility (Ohsawa et al., 2000, 2004), functions that require large amounts of cortical F-actin. Our immunocytochemical observations showed that ramified cells (characterized by larger TI values) that displayed minimal or no ruffling at all had only modest quantities of CaM proteins in the cell cortex as compared with ameboid or reactive microglia. Coincidentally, the amount of cortical F-actin was likewise less in ramified microglia, and the reorganization of the actin cytoskeleton determined the intracellular distribution of CaM. Concomitantly increased levels of Iba1 and CaM protein expression, however,

were evident both in unchallenged ameboid and in LPS- or LPS and CaM inhibitor-challenged, e.g. activated/reactive microglia. Our observations relating to the intracellularly redistributed CaM *vs.* F-actin are consistent with the findings in mast cells in previous studies. For example, Sullivan et al. (2000) demonstrated that CaM promoted the disassembly of cortical F-actin, while Psatha et al. (2004) found that the disassembly of the actin cytoskeleton eliminated CaM localization.

LPS activation renders microglia ameboid, induces several pro- and anti-inflammatory signaling molecules (Lim et al., 2015; Zhu et al., 2014) and neurotoxic substances through binding to the CD14/MD-2/Toll-like receptor 4-complex (Fricker et al., 2012; Tokes et al., 2011), and gives rise, among others, to cell spreading by interfering with the organization of the actin cytoskeleton through the alteration of integrin clustering (Abram and Lowell, 2009). Microglia activation was shown to involve the signaling pathways nuclear factor κB and p38 mitogen-activated protein kinase (Bachstetter et al., 2007; Cao et al., 2014; Kaushal et al., 2007). It must be noted, however, that the activation of microglial cells by LPS is not proliferative (Suzumura et al., 1991).

In our studies, LPS challenge did not display a significant effect on microglial cell survival or CaM and Iba1 protein expression, but resulted in significant cell spreading, documented in increases in cell surface, perimeter and TI, and in a repositioning of intracellular actin filaments toward podosome and filipodia formation. In spite of this lack of interaction between the LPS challenge and CaM protein expression, some of the effects of LPS are mediated through CaM-related phenomena in macrophages (Sweet and Hume, 1996). An LPS challenge, for example, elevated the intracellular Ca^{2+} concentration in brain macrophages via the activation of phosphatidylinositol (3,4,5)-trisphosphate-sensitive stores that, in turn, activated the actin cytoskeleton (Bader et al., 1994). Such an inflammatory response was recently identified as one developed through the activation of CaM-dependent kinase kinase 2 via Toll-like receptors (Racioppi et al., 2012). Thus, the effects of LPS could be attributed, at least in part, to CaM-related phenomena regulating the actin cytoskeleton without directly affecting the CaM protein expression. In another study, CaM was involved in spontaneous microglial ramification and the activation of proliferation from quiescence as it inhibited the spontaneous ramification and decreased the proliferation of these cells (Casal et al.,

2001). The loss of ramification was reported to be induced by the elevation of intracellular Ca^{2+} via direct or indirect routes (Kalla et al., 2003) that eventually resulted in CaM activation and/or accumulation in the cell cortex.

A number of studies demonstrated that cell cycle and proliferation could be regulated by CaM inhibitors (Berchtold et al., 2014; Borsa et al., 1986; Sunagawa et al., 2000). Borsa et al. (1986) compared the effects of CALMID and TFP in cycling and non-cycling cells and demonstrated that they were both preferentially cytotoxic for cycling cells. Cell proliferation studies on the osteosarcoma cell line (Tseng et al., 2004), pancreatic beta-cell line cells (Hügl and Merger, 2007) and human lung cancer stem-like cells (Yeh et al., 2012) demonstrated that CaM inhibitors effectively inhibited cell division. TFP inhibited cancer stem cell tumor formation and growth through Wnt/beta-catenin signaling (Yeh et al., 2012) and cell migration (Finlayson and Freeman, 2009; Linxweiler et al., 2013), and was shown to induce apoptosis in human lung adenocarcinoma cell lines (Chen et al., 2009). In our proliferation studies, unstimulated microglia (subDIV4) exhibited a low PI value (2.5%) indicating the presence of only a few mitotically active cells. This value would not be considered a prognostic feature in a number of human cancer types (Brownhill et al., 2014; Yamaguchi et al., 2013). Proliferation was strongly inhibited by LPS and TFP as they reduced the number of Ki67-positive microglia very effectively. CALMID, however, had no effect on cell proliferation in unchallenged cultures, albeit it did have some inhibitory effect in LPS-treated cells. Cell viability was also similarly differentially affected as TFP was more effective than CALMID in inhibiting the survival of pure microglial cells.

Both CALMID and TFP were previously shown to inhibit CaM activity primarily by binding directly to the protein (Matsushima et al., 2000; Sunagawa et al., 2000). However, CALMID and TFP probably exert many of their actions not only via their binding to CaM, but also by interfering directly with a number of upstream (Qin et al., 2009) or downstream targets of CaM signaling (James et al., 2009; Sunagawa et al., 2000). For example, the Rho family GTPases, e.g. Cdc42, Rac and Rho, are known to be intracellular switches that regulate remodeling of the actin cytoskeleton (Hall, 1998). They participate in membrane ruffling, lamellipodia and podosome formation and phagocytosis (Dovas et al., 2009; Kanazawa et al., 2002; Seasholtz et al., 2004). As recent studies led to the consculsion that CaM can regulate

the activation of both Rac1 and Cdc42 in megakaryocytes and platelets (Elsaraj and Bhullar, 2008; Xu and Bhullar, 2011; Xu et al., 2012), a direct involvement of CaM in cytoskeleton remodeling was established. By acting on a number of proteins simultaneously, these CaM antagonists could therefore have more complex effects, which differ from each other and may involve several signaling pathways, thereby further impairing a number of cellular functions. Taken together, these features could explain the differences seen in the efficacies of these CaM inhibitors as concerns various aspects of microglial morphology and function.

The ability of CaM to activate many target proteins depends on its highly flexible conformation, enabling it to interact with a wide variety of proteins (Yamniuk and Vogel, 2004). We hypothesize that this conformational flexibility is limited to different degrees when CaM inhibitors are applied; consequently, many of the CaM-regulated effects will be differentially affected by CaM inhibition. Thus, given the number of CaM-interacting target proteins and their participation in the various intracellular signaling pathways involved in, for example, the remodeling of the actin cytoskeleton during lamellipodia, filipodia or podosome formation (Evans et al., 2003; Murphy and Courtneidge, 2011; Sunagawa et al., 2000; Vincent et al., 2012), cell migration or phagocytosis (Sierra et al., 2013), it is difficult at present to give an accurate explanation as to how different CaM antagonists might interfere with the outcome of the signaling processes. It seems clear, however, that CaM inhibition interferes strongly with both morphological and functional aspects of the microglial cells. Future experiments may shed light on whether the effects of CaM inhibition seen in selected morphological and functional properties of microglia are uniquely characteristic of these cells or may perhaps be typical of other cell types too, and may promote an understanding of the cell type-specific roles of CaM.

5. Conclusion

CaM is a key factor in the regulation of a number of morphological aspects of the microglia through the modulation of the actin cytoskeleton that affects the formation and maintenance of lamellipodia, filipodia and podosomes of these cells. Acting on many target proteins, among which actin is of paramount importance, it regulates several cellular functions such as phagocytosis, cell proliferation and

survival. CALMID and TFP, two prototypical CaM antagonists acting through different molecular mechanisms on the CaM protein, have differential effects on these morphological and fuctional aspects, including Iba1 and CaM protein expression, when tested both in unchallenged and LPS-challenged pure microglial cells. In general, TFP was more potent in provoking these structural alterations and functional changes. Dechipering the roles of CaM in microglial functions, perhaps through use of different CaM-specific inhibitors, could be important in understanding the roles and modes of action of microglia in health and disease.

Acknowledgements

We thank Mrs. Susan Ambrus for excellent technical help and Ms. Diana Kata for helpful discussions. This work was supported by program project grants to the University of Szeged from the Hungarian Ministry of National Resources (TÁMOP-4.2.1.B-09/1/KONV-2010-0005 and TÁMOP-4.2.2.A-11/1/KONV-2012-0052) through the European Union Cohesion Fund to KG. The funders had no role in the study design, the data collection and analysis, the decision to publish, or the preparation of the manuscript.

Author Contributions

Conceived and designed the experiments: KG, MS. Performed the experiments: MS, KD. Analyzed the data: MS, KD. Contributed reagents/materials/analysis tools: KG. Wrote the paper: KG, MS. Edited the paper: KG.

Conflict of interest

The authors have declared that no competing interests exist.

References

Abram, C.L., and Lowell, C.A. (2009). The ins and outs of leukocyte integrin signaling. Annu. Rev. Immunol. 27, 339–362.

Ahmed, Z., Shaw, G., Sharma, V.P., Yang, C., McGowan, E., and Dickson, D.W. (2007). Actin-binding proteins coronin-1a and IBA-1 are effective microglial markers for immunohistochemistry. J. Histochem. Cytochem. 55, 687-700.

Bachstetter, A.D., Xing, B., de Almeida, L., Dimayuga, E.R., Watterson, D.M., Van Eldik, L.J. (2011). Microglial p38α MAPK is a key regulator of proinflammatory cytokine up-regulation induced by toll-like receptor (TLR) ligands or beta-amyloid (Aβ). J. Neuroinflammation 8, 79.

Bader, M.F., Taupenot, L., Ulrich, G., Aunis, D., and Ciesielski-Traska, J. (1994). Bacterial endotoxin induces [Ca2+]i transients and changes the organization of actin in microglia. Glia 11, 336–344.

Bakota, L., Orojan, I., and Gulya, K. (2005) Intranuclear differences in calmodulin gene expression in the trigeminal nuclei of the rat. Acta Biol. Szeged. 49, 9-14.

Berchtold, M.W., and Villalobo, A. (2014). The many faces of calmodulin in cell proliferation, programmed cell death, autophagy, and cancer. Biochim. Biophys. Acta 1843, 398-435.

Berridge, M.J., Lipp, P., and Bootman, M.D. (2000). The versatility and universality of calcium signalling. Nature Rev. Mol. Cell. Biol. 1, 11-21.

Borsa, J., Einspenner, M., Sargent, M.D., and Hickie, R.A. (1986). Selective cytotoxicity of calmidazolium and trifluoperazine for cycling versus noncycling C3H10T1/2 cells in vitro. Cancer Res. 46, 133-136.

Brownhill, S., Cohen, D., and Burchill, S. (2014). Proliferation index: A continuous model to predict prognosis in patients with tumours of the Ewing's sarcoma family. PLoS One 9, e104106.

Caceres, A., Bender, P., Snavely, L., Rebhun, L.I., and Steward, O. (1983). Distribution and subcellular localization of calmodulin in adult and developing brain tissue. Neuroscience 10, 449-461.

Cao, H., Zang, K.K., Han, M., Zhao, Z.Q., Wu, G.C., Zhang, Y.Q. (2014). Inhibition of p38 mitogen-activated protein kinase activation in the rostral anterior cingulate cortex attenuates pain-related negative emotion in rats. Brain Res. Bull. 107, 79-88.

Casal, C., Tusell, J.M., and Serratosa, J. (2001). Role of calmodulin in the differentiation/activation of microglial cells. Brain Res. 902, 101-107.

Chen, Q.Y., Wu, L.J., Wu, Y.Q., Lu, G.H., Jiang, Z.Y., Zhan, J.W., Jie, Y., and Zhou, J.Y. (2009). Molecular mechanism of trifluoperazine induces apoptosis in human A549 lung adenocarcinoma cell lines. Mol. Med. Report 2, 811–817.

Clapham, D.E. (2007). Calcium signaling. Cell 131, 1047-1058.

Dovas, A., Gevrey, J.C., Grossi, A., Park, H., Abou-Kheir, W., and Cox, D. (2009). Regulation of podosome dynamics by WASp phosphorylation: implication in matrix degradation and chemotaxis in macrophages. J. Cell Sci. 122, 3873-3882.

Drew, P.D., and Chavis, J.A. (2000). Inhibition of microglial cell activation by cortisol. Brain Res. Bull. 52, 391-396.

Elsaraj, S.M., and Bhullar, R.P. (2008). Regulation of platelet Rac1 and Cdc42 activation through interaction with calmodulin. Biochim. Biophys. Acta 1783, 770-778.

Erondu, N.E., and Kennedy, M.B. (1985). Regional distribution of type II Ca^{2+}/calmodulin-dependent protein kinase in rat brain. J. Neurosci. 5, 3270-3277.

Evans, J.G., Correia, I., Krasavina, O., Watson, N., and Matsudaira, P. (2003). Macrophage podosomes assemble at the leading lamella by growth and fragmentation. J. Cell Biol. 161, 697-705.

Färber, K., and Kettenmann, H. (2006). Functional role of calcium signals for microglial function. Glia 54, 656-665.

Finlayson, A.E., and Freeman, K.W. (2009). A cell motility screen reveals role for MARCKS-related protein in adherens junction formation and tumorigenesis. PLoS One 4, e7833.

Fricker, M., Oliva-Martín, M.J., and Brown, G.C. (2012). Primary phagocytosis of viable neurons by microglia activated with LPS or Aβ is dependent on calreticulin/LRP phagocytic signalling. J. Neuroinflammation 9, 196.

Fujita, H., Tanaka, J., Toku, K., Tateishi, N., Suzuki, Y., Matsuda S, Sakanaka M, and Maeda N. (1996). Effects of GM-CSF and ordinary supplements on the ramification of microglia in culture: A morphometrical study. Glia 18, 269-281.

Ginhoux, F., Greter, M., Leboeuf, M., Nandi, S., See, P., Gokhan S, Mehler MF, Conway SJ, Ng LG, Stanley ER, Samokhvalov IM, and Merad M. (2010). Fate mapping analysis reveals that adult microglia derive from primitive macrophages. Science 330, 841-845.

Greenberg, S. (1995). Signal transduction of phagocytosis. Trends Cell Biol. 5, 93-99.

Hall, A. (1998). Rho GTPases and the actin cytoskeleton. Science 279, 509-514.

Hügl, S.R., and Merger, M. (2007). Prolactin stimulates proliferation of the glucose-dependent beta-cell line INS-1 via different IRS-proteins. J. Pancreas 8, 739-752.

Ikura, M. (1996). Calcium binding and conformational response in EF-hand proteins. Trends Biochem. 21, 14-17.

Imai, Y., Ibata, I., Ito, D., Ohsawa, K., and Kohsaka, S. (1996). A novel gene iba1 in the major histocompatibility complex class III region encoding an EF hand protein expressed in a monocytic lineage. Biophys. Biochem. Res. Commun. 224, 855-862.

James, L.R., Griffiths, C.H., Garthwaite, J., and Bellamy, T.C. (2009). Inhibition of nitric oxide-activated guanylyl cyclase by calmodulin antagonists. Br. J. Pharmacol. 158, 1454-1464.

Kalla, R., Bohatschek, M., Kloss, C.U., Krol, J., Von Maltzan, X., and Raivich G. (2003). Loss of microglial ramification in microglia-astrocyte cocultures: involvement of adenylate cyclase, calcium, phosphatase, and Gi-protein systems. Glia 41, 50-63.

Kanazawa, H., Ohsawa, K., Sasaki, Y., Kohsaka, S., and Imai, Y. (2002). Macrophage/microglia-specific protein Iba1 enhances membrane ruffling and

Rac activation via phospholipase C-gamma -dependent pathway. J Biol. Chem. 277, 20026-20032.

Kaushal, V., Koeberle, P.D., Wang, Y., Schlichter, L.C. (2007). The Ca2+-activated K+ channel KCNN4/KCa3.1 contributes to microglia activation and nitric oxide-dependent neurodegeneration. J. Neurosci. 27, 234-244.

Kennedy, M.B. (1989). Regulation of neuronal function by calcium. Trends Neurosci. 12, 417-420.

Kortvely, E., and Gulya, K. (2004). Calmodulin, and various ways to regulate its activity. Life Sci. 74, 1065-1070.

Kortvely, E., Palfi, A., Bakota, L., and Gulya, K. (2002). Ontogeny of calmodulin gene expression in rat brain. Neuroscience 114, 301-316.

Kortvely, E., Varszegi, S., Palfi, A., and Gulya, K. (2003). Intracellular targeting of calmodulin mRNAs in primary hippocampal cells. J. Histochem. Cytochem. 51, 541-544.

Kovacs, B., and Gulya, K. (2002). Differential expression of multiple calmodulin genes in cells of the white matter of the rat spinal cord. Mol. Brain Res. 102, 28-34.

Kovacs, B., and Gulya, K. (2003). Calmodulin gene expression in the neural retina of the adult rat. Life Sci. 73, 3213-3224.

Kreutzberg, G.W. (1996). Microglia: A sensor for pathological events in the CNS. Trends Neurosci. 19, 312-318.

Libich, D.S., and Harauz, G. (2008). Backbone dynamics of the 18.5 kDa isoform of myelin basic protein reveals transient alpha-helices and a calmodulin-binding site. Biophys. J. 94, 4847-4866.

Lim, H.W., Park, J.I., More, S.V., Park, J.Y., Kim, B.W., Jeon, S.B., Yun, Y.S., Park, E.J., Yoon, S.H., Choi, D.K. (2015). Anti-neuroinflammatory effects of DPTP, a novel synthetic clovamide derivative in in vitro and in vivo model of neuroinflammation. Brain Res. Bull. 112, 25-34.

Linxweiler, M., Schorr, S., Schäuble, N., Jung, M., Linxweiler, J., Langer F, Schäfers HJ, Cavalié A, Zimmermann R, and Greiner M. (2013). Targeting cell migration and

the endoplasmic reticulum stress response with calmodulin antagonists: a clinically tested small molecule phenocopy of SEC62 gene silencing in human tumor cells. BMC Cancer 13, 574.

Lowry, O.H., Rosebrough, N.J., Farr, A.L., and Randall, R.J. (1951). Protein measurement with the Folin phenol reagent. J. Biol. Chem. 193, 265-275.

Matsushima, N., Hayashi, N., Jinbo, Y., and Izumi, Y. (2000). Ca^{2+}-bound calmodulin forms a compact globular structure on binding four trifluoperazine molecules in solution. Biochem. J. 347, 211-215.

Mitchison, T.J., and Cramer, L.P. (1996). Actin-based cell motility and cell locomotion. Cell 84, 371-379.

Murphy, D.A., and Courtneidge, S.A. (2011). The 'ins' and 'outs' of podosomes and invadopodia: characteristics, formation and function. Nature Rev. Mol. Cell Biol. 12, 413-426.

Myllykoski, M., Itoh, K., Kangas, S.M., Heape, A.M., Kang, S.U., Lubec G, Kursula I, and Kursula P. (2012). The N-terminal domain of the myelin enzyme 2',3'-cyclic nucleotide 3'-phosphodiesterase: direct molecular interaction with the calcium sensor calmodulin. J. Neurochem. 123, 515-524.

Ohsawa, K., Imai, Y., Kanazawa, H., Sasaki, Y., and Kohsaka, S. (2000). Involvement of Iba1 in membrane ruffling and phagocytosis of macrophages/microglia. J. Cell Sci. 113, 3073-3084.

Ohsawa, K., Imai, Y., Sasaki, Y., and Kohsaka, S. (2004). Microglia/macrophage-specific protein Iba1 binds to fimbrin and enhances its actin-bundling activity. J. Neurochem. 88, 844-856.

Orojan, I., Bakota, L., and Gulya, K. (2006). Differential calmodulin gene expression in the nuclei of the rat midbrain-brain stem region. Acta Histochem. 108, 455-462.

Orojan, I., Bakota, L., and Gulya, K. (2008). Trans-synaptic regulation of calmodulin gene expression after experimentally induced orofacial inflammation and subsequent corticosteroid treatment in the principal sensory and motor trigeminal nuclei of the rat. Neurochem. Int. 52, 265-271.

Palfi, A., and Gulya, K. (1999). Water deprivation upregulates the three calmodulin genes in exclusively the supraoptic nucleus of the rat brain. Mol. Brain Res. 74, 111-116.

Palfi, A. Kortvely, E., Fekete, E., and Gulya, K. (2005). Multiple calmodulin mRNAs are selectively transported to functionally different neuronal and glial compartments in the rat hippocampus. An electron microscopic in situ hybridization study. Life Sci. 77, 1405-1415.

Palfi, A., Kortvely, E., Fekete, E., Kovacs, B., Varszegi, S., and Gulya, K. (2002). Differential calmodulin gene expression in the rodent brain. Life Sci. 70, 2829-2855.

Palfi, A., Simonka, J.A., Pataricza, M., Tekulics, P., Lepran, I., Papp G, and Gulya K. (2001). Postischemic calmodulin gene expression in the rat hippocampus. Life Sci. 68, 2373-2381.

Palfi, A., Vizi, S., and Gulya, K. (1999). Differential distribution and intracellular targeting of mRNAs corresponding to the three calmodulin genes in rat brain: a quantitative in situ hybridization study. J. Histochem. Cytochem. 47, 583-600.

Prinz, M., and Priller, J (2014). Microglia and brain macrophages in the molecular age: from origin to neuropsychiatric disease. Nature Rev. Neurosci. 15, 300-312.

Psatha, M., Koffer, A., Erent, M., Moss, S.E., and Bolsover, S. (2004). Calmodulin spatial dynamics in RBL-2H3 mast cells. Cell Calcium 36, 51-59.

Qin, J., Zima, A.V., Porta, M., Blatter, L.A., and Fill, M (2009). Trifluoperazine: a ryanodine receptor agonist. Pflugers Arch. 458, 643-651.

Racioppi, L., Noeldner, P.K., Lin, F., Arvai, S., and Means, A.R. (2012). Calcium/calmodulin-dependent protein kinase kinase 2 regulates macrophage-mediated inflammatory responses. J. Biol. Chem. 287, 11579-11591.

Rotty, J.D., Wu, C., and Bear, J.E. (2013). New insights into the regulation and cellular functions of the ARP2/3 complex. Nature Rev. Mol. Cell Biol. 14, 7-12.

Sacks, D.B., Porter, S.E., Ladenson, J.H., and McDonald, J.M. (1991). Monoclonal antibody to calmodulin: development, characterization, and comparison with polyclonal anti-calmodulin antibodies. Anal. Biochem. 194, 369-377.

Saijo, K., and Glass, C.K. (2011). Microglial cell origin and phenotypes in health and disease. Nature Rev. Immunol. 11 775-787.

Sanabria, H., Digman, M.A., Gratton, E., and Waxham, M.N. (2008). Spatial diffusivity and availability of intracellular calmodulin. Biophys. J. 95, 6002-6015.

Scott, I.S., Heath, T.M., Morris, L.S., Rushbrook, S.M., Bird, K., Vowler, S.L., Arends, M.J., and Coleman, N. (2004). A novel immunohistochemical method for estimating cell cycle phase distribution in ovarian serous neoplasms: implications for the histopathological assessment of paraffin-embedded specimens. Br. J. Cancer 90, 1583-1590.

Seasholtz TM, Radeff-Huang J, Sagi SA, Matteo R, Weems JM, Cohen AS, Feramisco JR, and Brown JH. (2004). Rho-mediated cytoskeletal rearrangement in response to LPA is functionally antagonized by Rac1 and PIP2. J. Neurochem. 91, 501-512.

Seto-Ohshima, A., Kitajima, S., Sano, M., Kato, K., and Mizutani, A. (1983). Immunohistochemical localization of calmodulin in mouse brain. Histochemistry 79, 251-257.

Siddiqui, T.A., Lively, S., Vincent, C., and Schlichter, L.C. (2012). Regulation of podosome formation, microglial migration and invasion by $Ca(^{2+})$-signaling molecules expressed in podosomes. J. Neuroinflammation 9, 250.

Sierra, A., Abiega, O., Shahraz, A., and Neumann, H. (2013). Janus-faced microglia: beneficial and detrimental consequences of microglial phagocytosis. Front. Cell. Neurosci. 7, 6.

Solá, C., Tusell, J.M., and Serratosa, J. (1996). Comparative study of the pattern of expression of calmodulin messenger RNAs in the mouse brain. Neuroscience 75, 245-256.

Solá, C., Tusell, J.M., and Serratosa, J. (1997). Calmodulin is expressed by reactive microglia in the hippocampus of kainic acid-treated mice. Neuroscience 81, 699-705.

Song, X.Y., Hu, J.F., Sun, M.N., Li, Z.P., Zhu, Z.X., Song, L.K., Yuan, Y.H., Liu, G., Chen, N,H. (2014). IMM-H004, a novel coumarin derivative compound, attenuates the production of inflammatory mediatory mediators in lipopolysaccharide-activated BV2 microglia. Brain Res. Bull. 106, 30-38.

Strack, S., Wadzinski, B.E., and Ebner, F.F. (1996). Localization of the calcium/calmodulin-dependent protein phosphatase, calcineurin, in the hindbrain and spinal cord of the rat. J. Comp. Neurol. 375, 66-76.

Streit, W.J., Walter, S.A., and Pennel, N.A. (1999). Reactive microgliosis. Progr. Neurobiol. 57, 563-581.

Sullivan, R., Burnham, M., Török, K., and Koffer, A. (2000). Calmodulin regulates the disassembly of cortical F-actin in mast cells but is not required for secretion. Cell Calcium 28, 33-46.

Sunagawa, M., Kosugi, T., Nakamura, M., and Sperelakis, N (2000). Pharmacological actions of calmidazolium, a calmodulin antagonist, in cardiovascular system. Cardiovasc. Drug Rev. 18, 211-221.

Suzumura, A., Marunouchi, T., and Yamamoto, H (1991). Morphological transformation of microglia in vitro. Brain Res. 545, 301–306.

Sweet, M.J., and Hume, D.A. (1996). Endotoxin signal transduction in macrophages. J. Leukoc. Biol. 60, 8-26.

Szabo, M., and Gulya, K. (2013). Development of the microglial phenotype in culture. Neuroscience 241, 280-295.

Tokes, T., Eros, G., Bebes, A., Hartmann, P., Várszegi, S., Varga, G., Kaszaki, J., Gulya, K., Ghyczy, M., and Boros, M. (2011). Protective effects of a phosphatidylcholine-enriched diet in lipopolysaccharide-induced experimental neuroinflammation in the rat. Shock 36, 458-465.

Toutenhoofd, S.L., and Strehler, E.E. (2000). The calmodulin multigene family as a unique case of genetic redundancy: multiple levels of regulation to provide spatial and temporal control of calmodulin pools? Cell Calcium 28, 83-96.

Town, T., Nikolic, V., and Tan, J. (2005). The microglial "activation" continuum: from innate to adaptive responses. J. Neuroinflammation 2, 24.

Tseng, L.L., Huang, C.J., Hsu, S.S., Chen, J.S., Cheng, H.H., Chang HT, Jiann BP, and Jan C.R. (2004). Effect of calmidazolium on Ca($^{2+}$) movement and proliferation in human osteosarcoma cells. Clin. Exp. Pharmacol. Physiol. 31, 732-737.

Vandonselaar, M., Hickie, R.A., Quail, J.W., and Delbaere, L.T. (1994). Trifluoperazine-induced conformational change in Ca($^{2+}$)-calmodulin. Nature Struct. Biol. 1, 795-801.

Vertessy, B.G., Harmat, V., Bocskei, Z., Naray-Szabo, G., Orosz. F., and Ovadi, J. (1998). Simultaneous binding of drugs with different chemical structures to Ca^{2+}-calmodulin: crystallographic and spectroscopic studies. Biochemistry 37, 15300-15310.

Vincent, C., Siddiqui, T.A., and Schlichter, L.C. (2012). Podosomes in migrating microglia: components and matrix degradation. J. Neuroinflammation 9, 190.

Vizi, S., Palfi, A., and Gulya, K. (2000). Multiple calmodulin genes exhibit systematically differential responses to chronic ethanol treatment and withdrawal in several regions of the rat brain. Mol. Brain Res. 83, 63-71.

Wong, R., Schlichter, L.C. (2014). PKA reduces the rat and human KCa3.1 current, CaM binding, and Ca2+ signaling, which requires Ser332/334 in the CaM-binding C terminus. J. Neurosci. 34, 13371-13383.

Wu, Y., Wu, M., He, G., Zhang, X., Li, W., Gao, Y., Li, Z., Wang, Z., and Zhang, C. (2012). Glyceraldehyde-3-phosphate dehydrogenase: a universal internal control for Western blots in prokaryotic and eukaryotic cells. Anal. Biochem. 423, 15-22.

Xu, B., and Bhullar, R.P. (2011). Regulation of Rac1 and Cdc42 activation in thrombin- and collagen-stimulated CHRF-288-11 cells. Mol. Cell. Biochem. 353, 73-79.

Xu, B., Chelikani, P., and Bhullar, R.P. (2012). Characterization and functional analysis of the calmodulin-binding domain of Rac1 GTPase. PLoS One 7, e42975.

Yamada, M., Ohsawa, K., Imai, Y., Kohsaka, S., and Kamitori, S. (2006). X-ray structures of the microglia/macrophage-specific protein Iba1 from human and mouse demonstrate novel molecular conformation change induced by calcium binding. J. Mol. Biol. 364, 449-457.

Yamaguchi, T., Fujimori, T., Tomita, S., Ichikawa, K., Mitomi, H., Ohno, K., Shida, Y., and Kato, H. (2013). Clinical validation of the gastrointestinal NET grading system: Ki67 index criteria of the WHO 2010 classification is appropriate to predict metastasis or recurrence. Diagn. Pathol. 8, 65.

Yamniuk, A.P., and Vogel, H.J. (2004). Calmodulin's flexibility allows for promiscuity in its interactions with target protein and peptides. Mol. Biotechnol. 27, 33–57.

Yeh, C.T., Wu, A.T., Chang, P.M., Chen, K.Y., Yang, C.N., Yang SC, Ho CC, Chen CC, Kuo YL, Lee PY, Liu YW, Yen CC, Hsiao M, Lu PJ, Lai JM, Wang LS, Wu CH, Chiou JF, Yang PC, and Huang CY. (2012). Trifluoperazine, an antipsychotic agent, inhibits cancer stem cell growth and overcomes drug resistance of lung cancer. Am. J. Respir. Crit. Care Med. 186, 1180-1108.

Zhu, M.D., Zhao, L.X., Wang, X.T., Gao, Y.J., Zhang, Z.J. (2014). Ligustilide inhibits microglia-mediated proinflammatory cytokines production and inflammatory pain. Brain Res. Bull. 109, 54-60.

Figure Captions

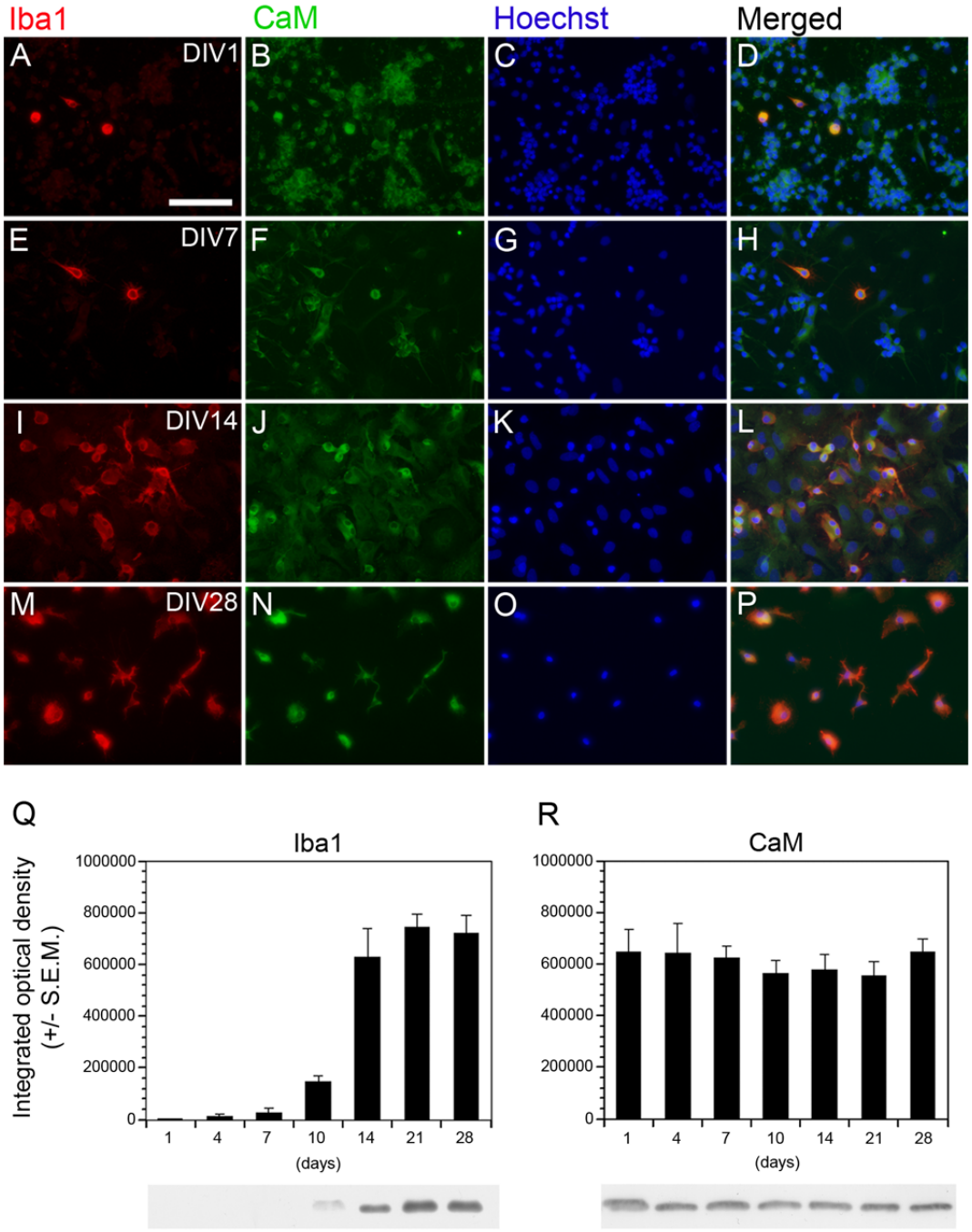

Figure 1. Development of Iba1 and CaM immunoreactivities in primary mixed cortical cultures (DIV1-DIV28). At early culturing times (DIV1 **(A-D)** and DIV7 **(E-H)**), all seeded cells displayed CaM immunoreactivity (green), but only a few of them were Iba1-positive microglia (red). The cell nuclei (blue) were labeled with Hoechst 33258. Since most of the cells present early in the culturing are neurons [48], most of the CaM immunoreactivity seen at DIV1-DIV7 is of neuronal origin. At DIV14 **(I-L)**, a large number of Iba1-positive cells showed CaM positivity, a number of them were ramified. At DIV28 **(M-P)**, the predominant cell type in the culture was the CaM-positive microglia. Note the visibly different Iba1 **(M)** and CaM contents **(N)** of the ameboid and ramified microglia at this culturing time. The merged pictures show cells double-positive for Iba1 and CaM **(D, H, L, P)**. The development of Iba1 **(Q)** and CaM **(R)** immunoreactivities during culturing (DIV1-DIV28) was quantitatively analyzed on Western blots. Protein samples from primary cultures were separated by gel electrophoresis, transferred to nitrocellulose membranes and probed with either the Iba1 (**Q**) or CaM (**R**) antibody. Gray scale digital images of the immunoblots were acquired by scanning the autoradiographic films with a desktop scanner. The images were scanned and processed at identical settings to allow comparisons between the Western blots from different samples. Error bars indicate integrated optical density values (mean ± S.E.M.). Representative Western blot pictures are shown below the graphs. During culturing (DIV1-DIV28), a massive increase in the number of cells with microglial phenotype was observed in the mixed primary cultures, while the CaM content of the cultures remained constant. Most of the gain in Iba1 content occurred between DIV10 and DIV14. Culturing times are indicated at the upper right corners **(A, E, I, M)**. Scale bar in **A** for all pictures: 50 μm.

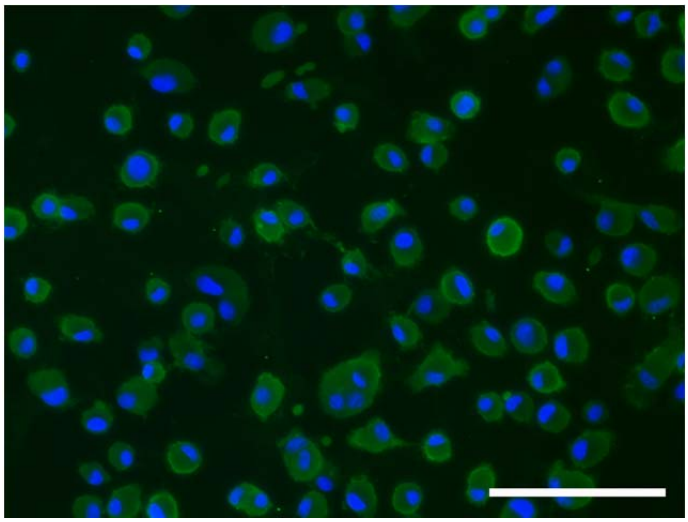

Figure 2. Localization of Iba1 immunoreactivity in pure microglial cell cultures (subDIV4). Representative photomicrograph of Iba1 imunoreactive microglial cells in culture. The purity of this culture is close to 100%, since every Hoechst 33258-labeled cell nuclei (blue) is surrounded by Iba1 immunopositive cytoplasm (green). Scale bar: 100 μm.

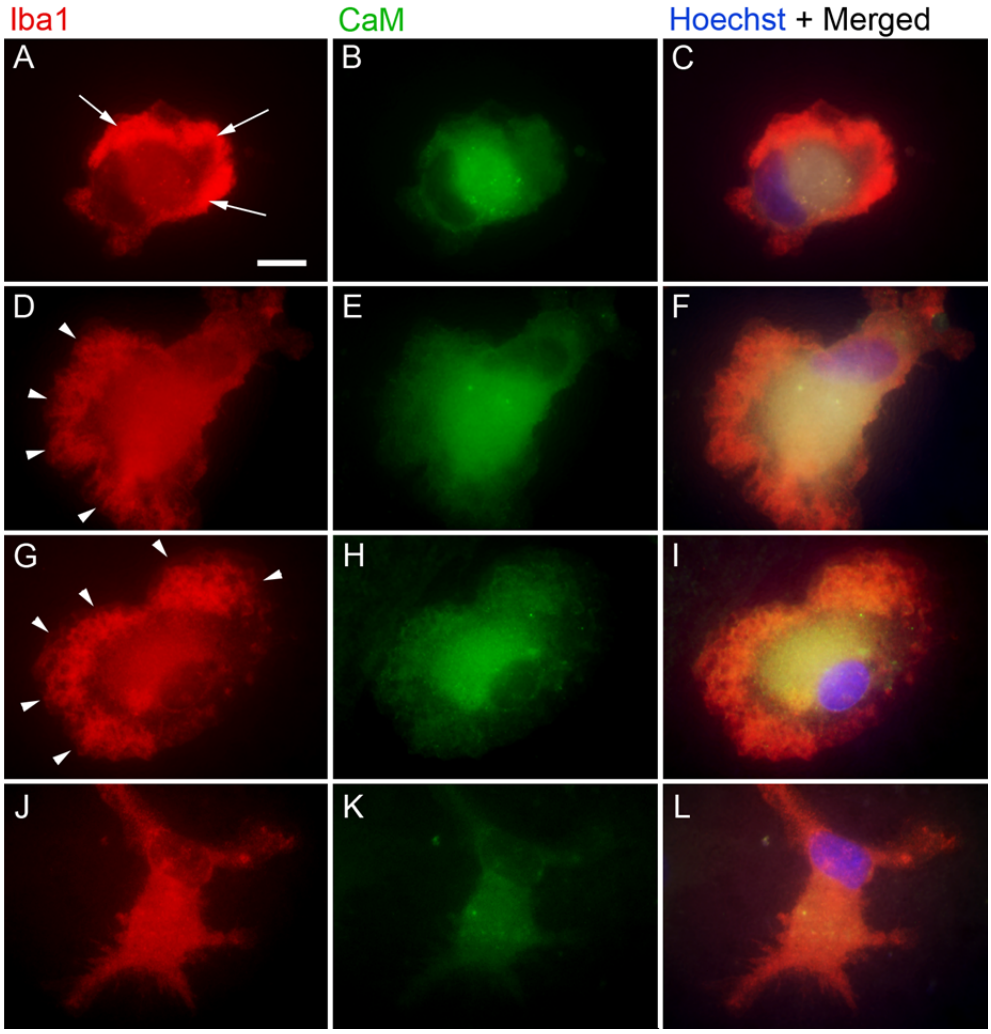

Figure 3. Distribution of Iba1 and CaM immunoreactivities in pure microglial cells (subDIV4). In pure microglial cultures (subDIV4), the majority of the unchallenged cells were ameboid or slightly ramified. While the Iba1 immunoreactivity (red) could be localized into two subcellular compartments, the perinuclear and the cell cortex domains **(A, D, G, J)**, the CaM immunoreactivity (green) was largely confined to the perinuclear region **(B, E, H, K)**, with the cell cortex having a considerably smaller CaM content, which progressively diminished deeper into the branches. Merged pictures **(C, F, I, L)** show the cell nuclei (blue) and the overlapping Iba1 and CaM immunoreactivities predominantly localized to the perinuclear area. Ameboid microglia have predominantly cortically localized Iba1 immunoreactivity in the leading edges of large lamellipodia (**A**, arrows), a cytoplasmic domain largely devoid of CaM immunoreactivity (**B**). Arrowheads **(D, G)** point to large lamellipodia. Scale bar in **A** for all pictures: 10 μm.

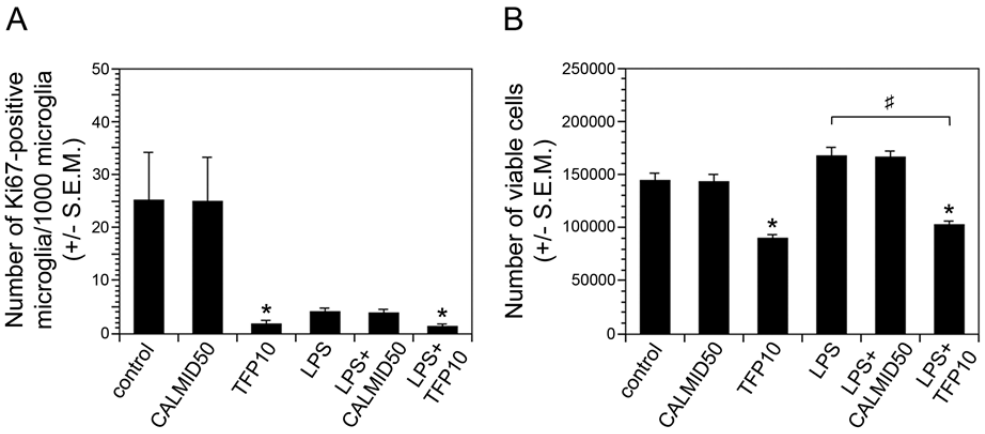

Figure 4. Effects of CaM inhibitors on microglia proliferation and viability in pure microglial cell cultures. The number of Ki67-positive microglia **(A)** and the viable cells **(B)** were quantitatively analyzed in challenged and untreated (control), LPS-challenged and LPS-challenged and treated cells. CALMID and TFP were tested at 50 nM and 10 μM, respectively, either alone or in combination with 100 ng/ml LPS. TFP, either alone or in combination with LPS, significantly decreased both microglia proliferation **(A)** and the number of viable cells **(B)** in the cultures (subDIV4). Interestingly, while the combined treatment of CALMID50 and LPS led to some (but not significant) inhibition on microglia proliferation, it was without any effect on cell viability. For proliferation studies, data (mean ± S.E.M.) were collected from at least 4 independently established cultures, each involving plating on at least 3 Petri dishes. Mean PI values (%) were established as follows: control = 2.52%, CALMID50 = 2.48%, TFP10 = 0.22%, LPS = 0.41%, LPS+CALMID50 = 0.20%, LPS+TFP10 = 0.12%. For viability studies, data (mean ± S.E.M.) were collected from at least 3 separate culturings, each involving plating on at least 6 Petri dishes. Data were analyzed with Kruskal-Wallis one-way ANOVA on ranks, followed by pairwise multiple comparisons (Dunn's method). *Statistically significant from control ($p<0.05$); #statistically significant from LPS-treated cells ($p<0.05$). LPS: 100 ng/ml; CALMID50: 50 nM CALMID; TFP10: 10 μM TFP.

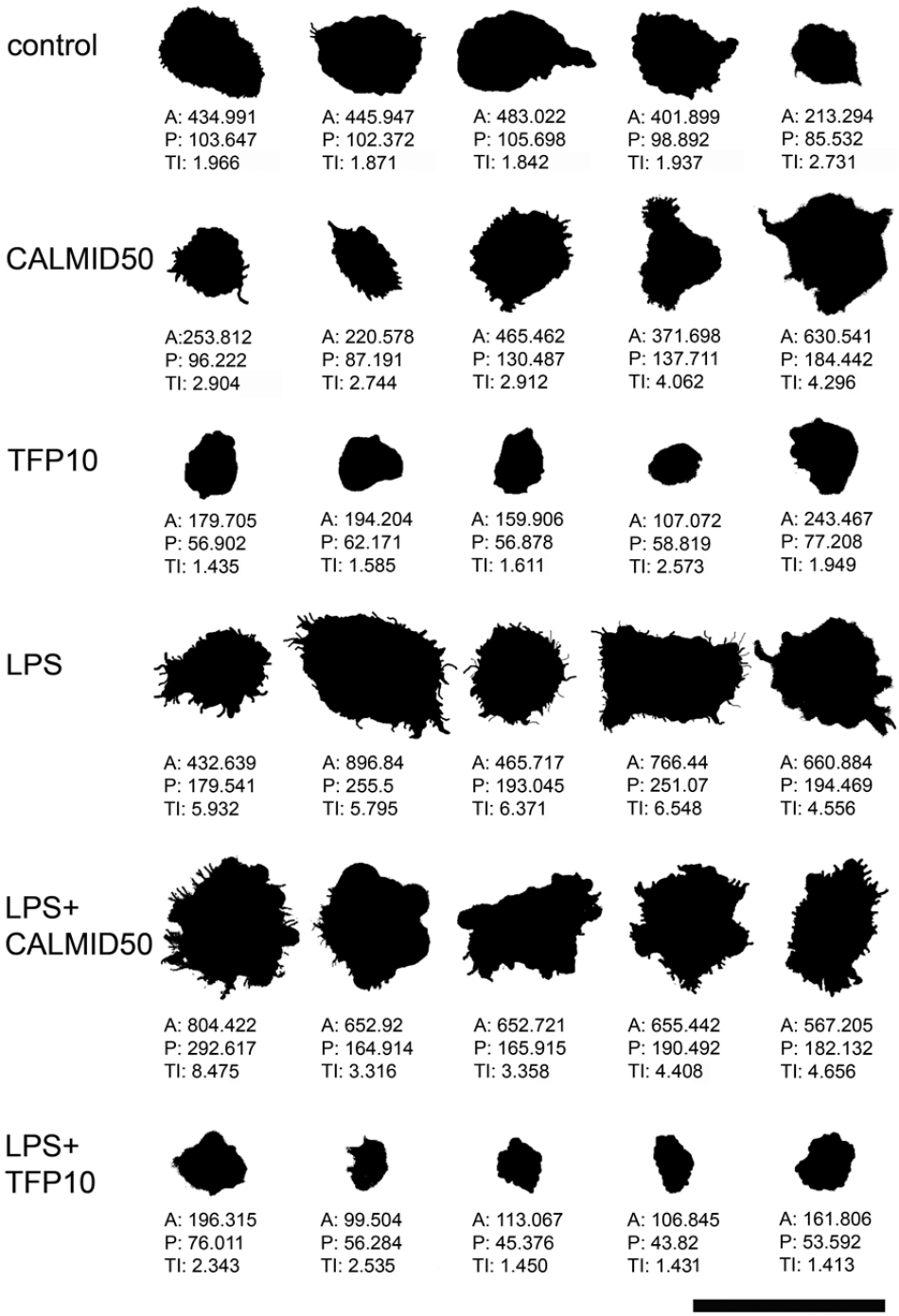

Figure 5. Representative binary silhouettes from pure microglial cultures after different treatment regimens. Iba1-positive microglial cells from pure microglial cultures (subDIV4) were photographed, digitized and quantitatively analyzed according to their morphological characteristics. Five representative binary silhouettes are shown at each culturing time. CALMID50, in either control or LPS-challenged microglia, increased the number of filipodia, while the complete absence of filipodia was seen both in TFP10 and in LPS+TFP10-treated microglia. Area (A) in μm^2, perimeter (P) in μm, and TI values (calculated as [perimeter of cell (μm)]^2/4π[cell area (μm^2)]) are indicated for each digitized cell. LPS: 100 ng/ml; CALMID50: 50 nM CALMID; TFP10: 10 μM TFP. Scale bar for all silhouettes: 50 μm.

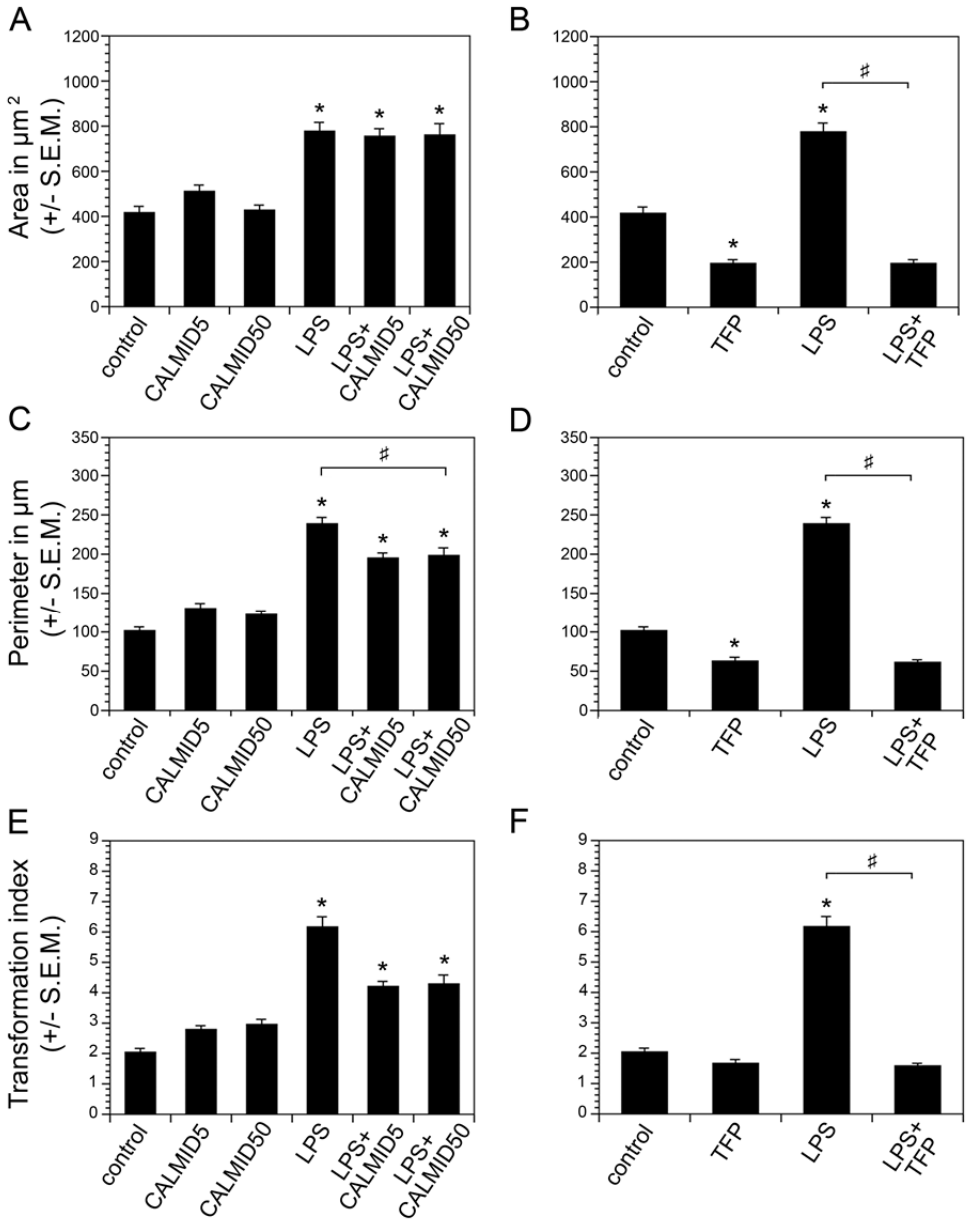

Figure 6. Effects of CaM inhibitors on selected morphological parameters of pure microglial cells. Surface area **(A, B)** in µm², perimeter **(C, D)** in µm, and TI values **(E, F)** of the microglia for CALMID **(A, C, E)** and TFP **(B, D, F)** were analyzed in pure unchallenged and LPS-challenged microglial cell cultures. All statistical comparisons were made by using SigmaPlot (v. 12.3, Systat Software Inc., Chicago, IL, USA) and analyzed with Kruskal-Wallis one-way analysis of variance, followed by Dunn's method for pairwise multiple comparison procedures for statistically significant differences between the groups. Values (mean ± S.E.M.) were computed from at least three independent culturing experiments. *Statistically significant from control ($p<0.05$); #statistically significant from LPS-treated cells. LPS: 100 ng/ml; CALMID5: 5 nM CALMID; CALMID50: 50 nM CALMID; TFP10: µM TFP.

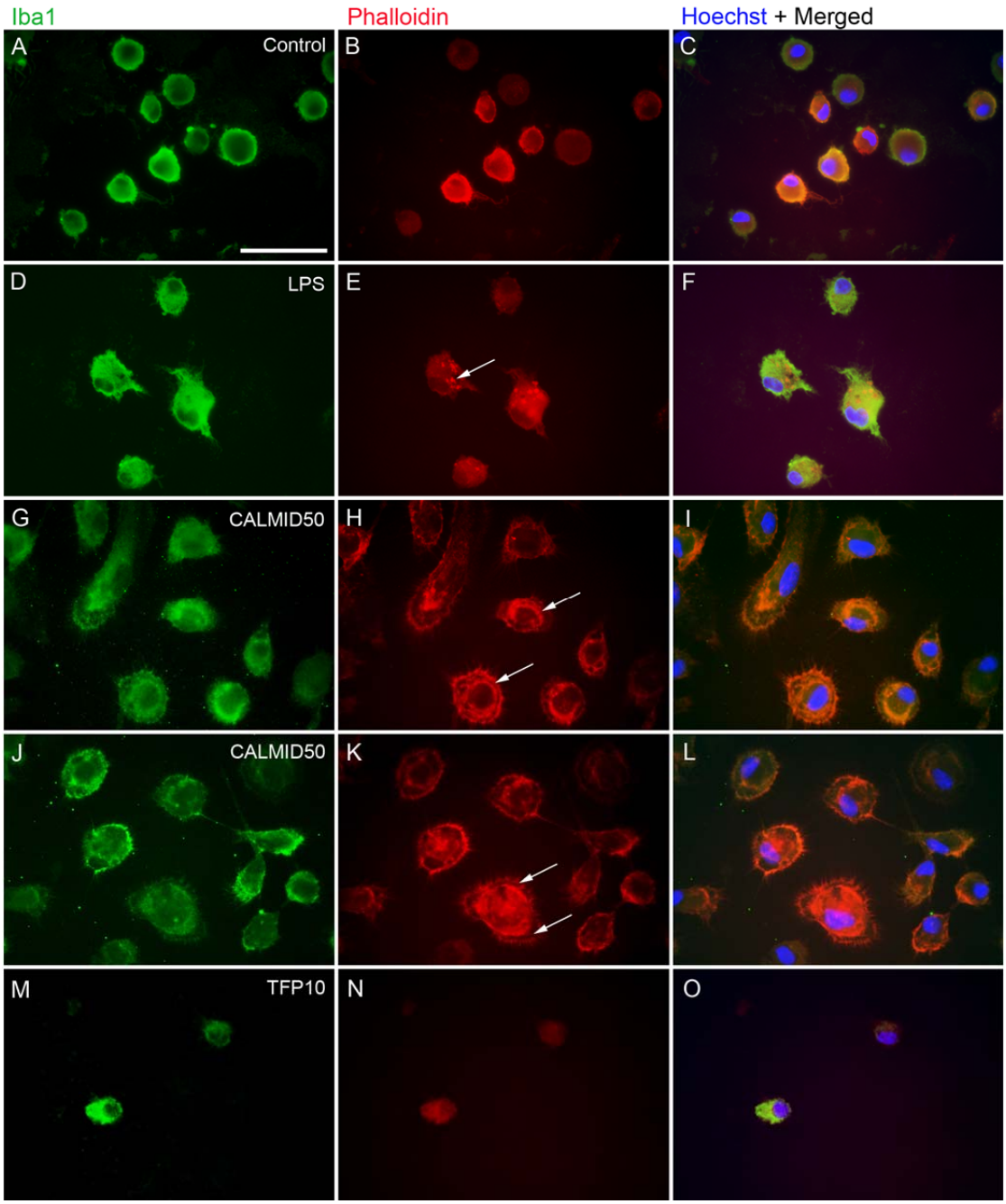

Figure 7. Immunocytochemical localization of actin-binding proteins in pure microglial cells. Iba1 immunoreactivity **(A, D, G, J, M**; shown here in green**)** and phalloidin fluorescence **(B, E, H, K, N**; shown in red**)** were colocalized in unchallenged and untreated (control) cells and in microglia treated with LPS or CaM inhibitors in pure microglial cultures (subDIV4). Merged pictures **(C, F, I, L, O)** show the Hoechst 33258-labeled cell nuclei (blue) and the colocalization of Iba1 immunoreactivity and phalloidin fluorescence. Filamentous actin often forms continuous ring-like lamellipodia in unchallenged microglia **(B)**. In LPS-challenged microglial cells, lamellipodia were less dominant, but the toxin stimulated podocyte formation, as indicated by several puncta delineated by phalloidin fluorescence **(**arrow, **E)**. When CALMID50 was used, strong lamellipodia formation was observed, often accompanied by a perinuclear cytoplasmic streaming of filamentous actin **(**arrows, **H, K)**, giving a double-ringed appearance of these cells. TFP treatment abolished the formation of filamentous actin bundles as detected by phalloidin fluorescence microscopy **(N)**. LPS: 100 ng/ml; CALMID50: 50 nM CALMID; TFP10: 10 μM TFP. Scale bar in panel **A** for all pictures: 50 μm.

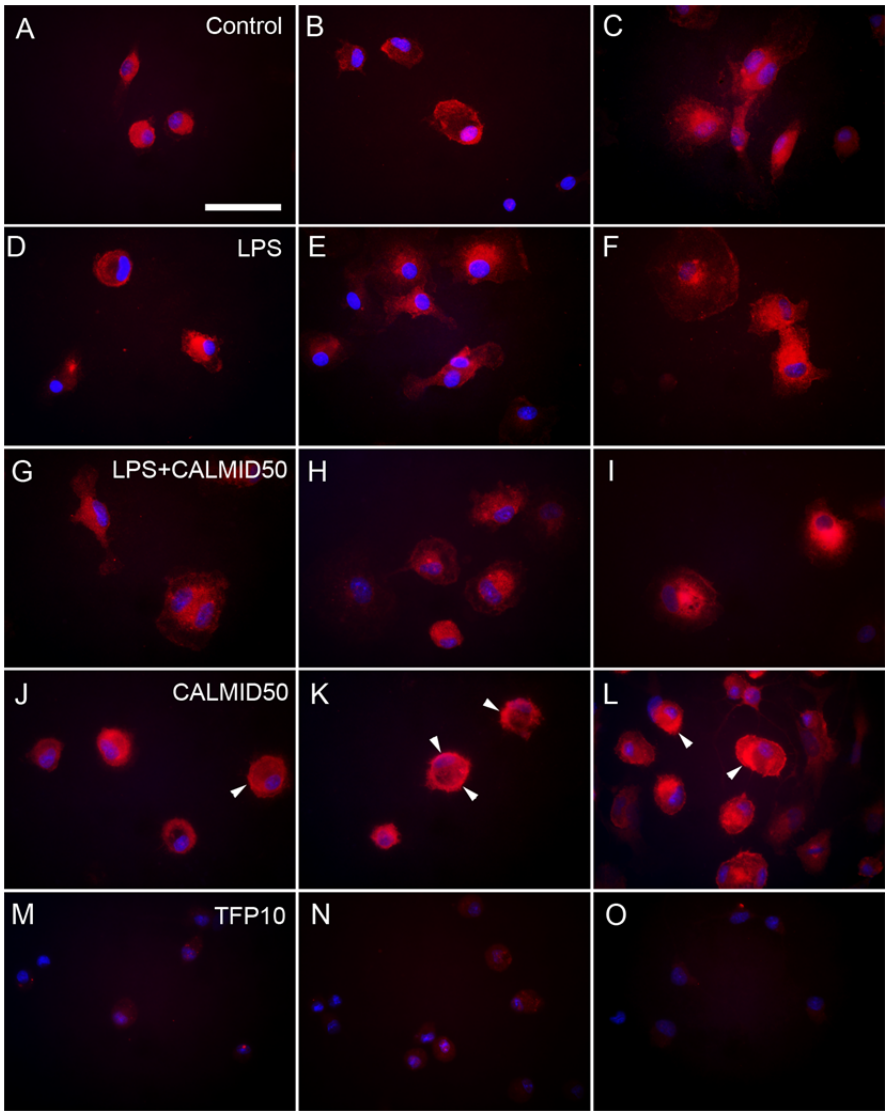

Figure 8. Effects of CaM inhibitors on the intracellular localization of CaM immunoreactivity in pure microglial cells. Representative immunocytochemical pictures showing the intracellular distribution of CaM immunopositivity (red) in pure microglia cells (subDIV4). The merged pictures show the cell nuclei (blue) that were stained with Hoechst 33258. The unchallenged and untreated (control) microglia (**A-C**) and LPS-challenged cells (**D-F**) showed mainly perinuclearly localized CaM immunoreactivity. LPS-challenged and treated cells (**G-I**), and more typically CALMID50-treated microglia (**J-L**) displayed CaM distribution often more targeted to the cell cortex and developing lamellipodia (arrowheads). TFP treatment resulted in a significant cell death (see Figure 4) and a homogenous cytoplasmic distribution of CaM immunoreactivity in the surviving microglia (**M-O**). LPS: 100 ng/ml; CALMID50: 50 nM CALMID; TFP10: 10 μM TFP. Scale bar in panel **A** for all pictures: 50 μm.

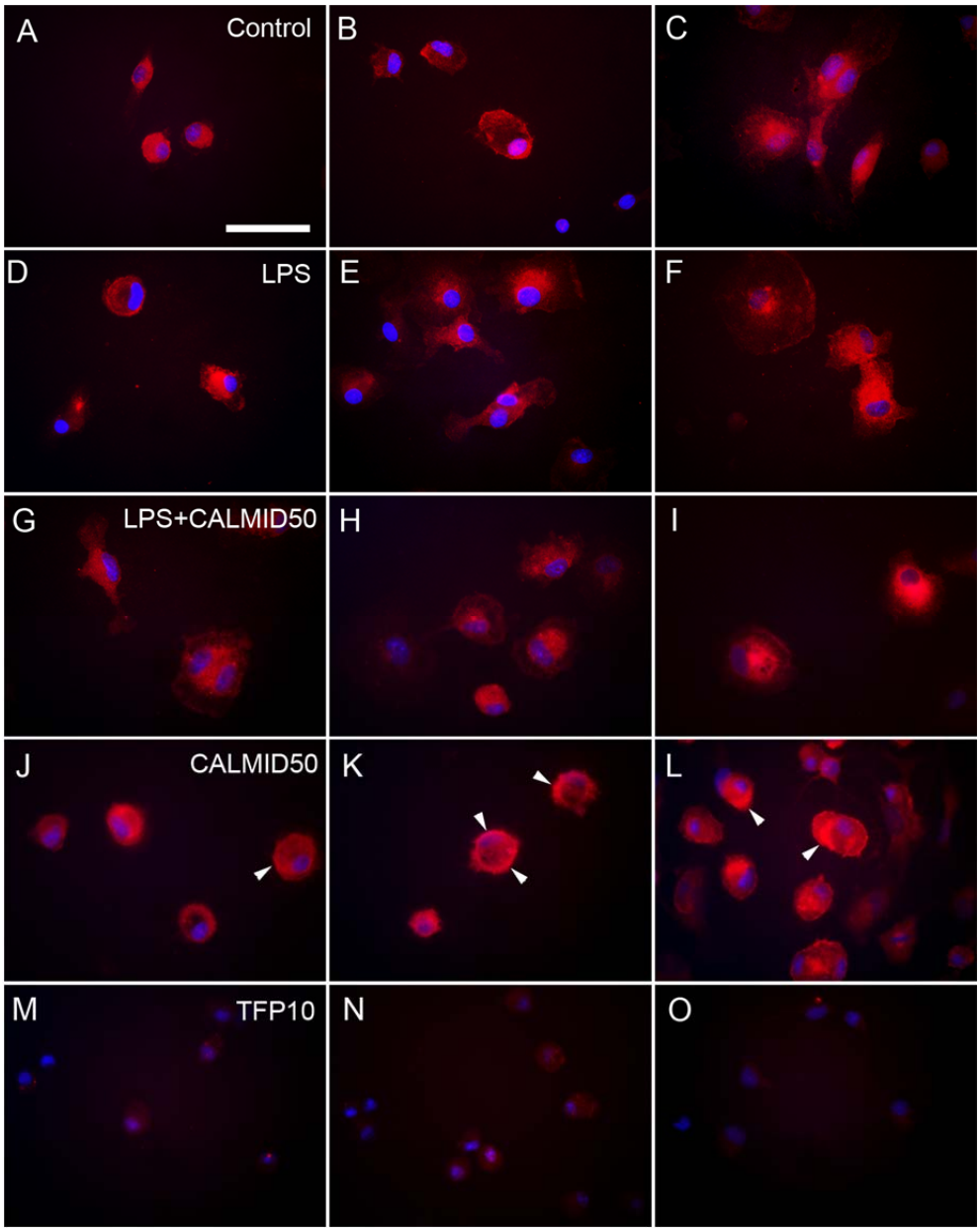

Figure 9. Effects of CaM inhibitors on Iba1 and CaM protein expression in pure microglial cells, as detected by Western blot analysis. Quantitative Western blot analysis of Iba1 (**A, C**) and CaM (**B, D**) immunoreactivities in pure microglial cell cultures (subDIV4). Representative Western blot pictures of the respective immunoreactivities are shown below the graphs together with the GAPDH immunoreactive bands that served as inner standards in the same gel. Protein samples were collected from 3 separate culturings, each involving plating on at least 6 Petri dishes, electrophoresed and quantitatively analyzed as described in the Materials and methods section. The integrated optical density data (mean ± S.E.M.), normalized to GAPDH immunoreactivities, were analyzed with Kruskal-Wallis one-way ANOVA on ranks, followed by pairwise multiple comparisons (Dunn's method). *Statistically significant from control ($p<0.05$); #statistically significant from LPS-treated cells. Iba1: ionized calcium-binding adaptor molecule 1; CaM: calmodulin; LPS: 100 ng/ml; CALMID5 and CALMID50: 5 and 50 nM CALMID; TFP10 and TFP20: 10 and 20 μM TFP; GAPDH: glyceraldehyde 3-phosphate dehydrogenase.

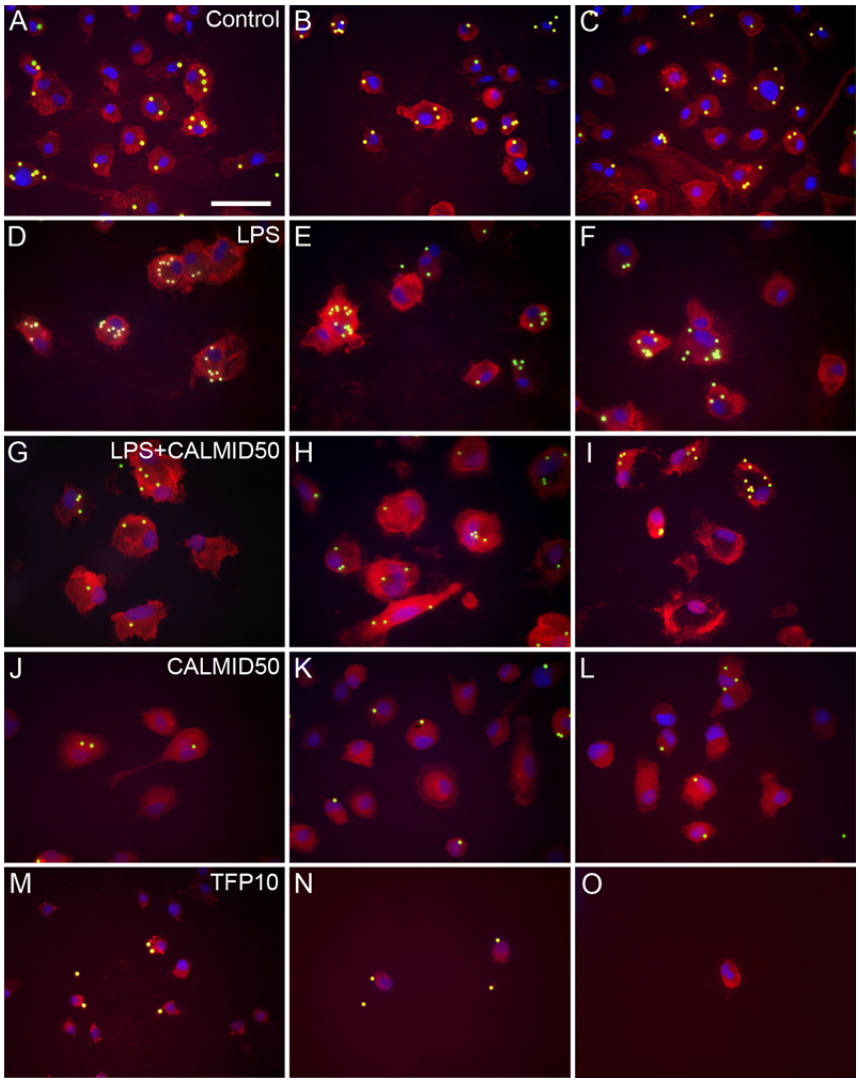

Figure 10. Effects of CaM inhibitors on the phagocytic activity of microglial cells in pure microglial cultures. Distribution of phagocytosed microbeads in pure microglial cultures. Representative pictures showing Iba1-immunopositive microglia demonstrate that the unstimulated and untreated (control) (**A-C**), LPS-challenged (**D-F**), LPS + CALMID50-treated **(G-I)**, CALMID50-treated (**J-L**) and TFP10-treated (**M-O**) microglia displayed different degrees of phagocytosis, as evidenced by the number of phagocytosed microbeads. Fluorescent dye-coated latex microbeads (d = 2 μm) (green) were added to the media and phagocytosed by microglial cells. After exposure to the fluorospheres, the culture was rinsed, the cells were formalin-fixed, labeled first with anti-Iba1 antibody (red), and then with Alexa Fluor fluorochrome-conjugated secondary antibody, and the cell nuclei (blue) were stained with Hoechst 33258. LPS: 100 ng/ml; CALMID50: 50 nM CALMID; TFP10: 10 μM TFP. Scale bar in panel **A** for all pictures: 50 μm.

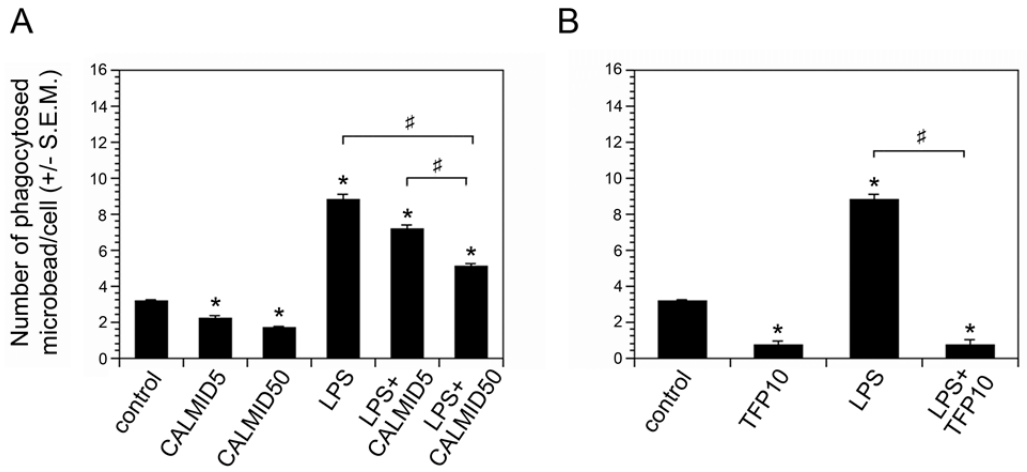

Figure 11. Effects of CaM inhibitors on the phagocytic activity of microglial cells in pure microglial cultures. Quantitative analysis of the number of phagocytosed microbeads after treatment with CALMID **(A)** or TFP **(B)** in unchallenged and in LPS-challenged microglial cells. For the study of the effects of CaM inhibitors on the number of phagocytosed beads (mean ± S.E.M.), a total of 873 bead-labeled cells were counted in three separate culturing procedures. Data were analyzed with Kruskal-Wallis one-way ANOVA on ranks, followed by pairwise multiple comparisons (Dunn's method). *Statistically significant from control ($p<0.05$); #statistically significant from LPS-treated cells. LPS: 100 ng/ml; CALMID5: 5 nM CALMID; CALMID50: 50 nM CALMID; TFP10: 10 μM TFP.

Tables

Table 1. Antibodies used in immunocytochemistry and Western blot analyses

Antibodies used in immunocytochemistry					
Primary antibody, abbrev. name	**Full name**	**Final dilution**	**Company name**	**Secondary antibody with fluorochrome**	**Final dilution**
Iba1	Rabbit anti-Iba1 monocl. ab.	1/300	Wako, Osaka, Japan	Alexa Fluor 568 goat anti-rabbit, Invitrogen, Carlsbad, CA, USA	1/1,000
Iba1	Rabbit anti-Iba1 monocl. ab.	1/300	Wako, Osaka, Japan	Alexa Fluor 488 goat anti-rabbit, Invitrogen, Carlsbad, CA, USA	1/1,000
CaM	Mouse anti-CaM, monocl. ab.	1/100	Millipore	Alexa Fluor 488 goat anti-mouse, Invitrogen, Carlsbad, CA, USA	1/1,000
CaM	Rabbit anti-CaM, monocl. ab., clone EP799Y	1/100	Abcam, Cambridge, UK	Alexa Fluor 568 goat anti-rabbit, Invitrogen, Carlsbad, CA, USA	1/1,000
Ki67	Rabbit anti-Ki67, monocl. ab., clone SP6	1/100	Thermo Scientific, Fremont, CA, USA	Alexa Fluor 488 goat anti-rabbit, Invitrogen, Carlsbad, CA, USA	1/1,000
Antibodies used in Western studies					
Primary antibody, abbrev. name	**Full name**	**Final dilution**	**Company name**	**Secondary antibody**	**Final dilution**
Iba1	Rabbit anti-Iba1 monocl. ab.	1/1,000	Wako, Osaka, Japan	Anti-rabbit IGG, peroxidase conjug., Sigma, St. Louis, MO, USA	1/2,000
CaM	Rabbit anti-CaM, monocl. ab., clone EP799Y	1/2,000	Abcam, Cambridge, UK	Anti-rabbit IGG, peroxidase conjug., Sigma, St. Louis, MO, USA	1/2,000
GAPDH	Mouse anti-GAPDH, monocl. ab., clone GAPDH-71.1	1/20,000	Sigma, St. Louis MO, USA	Anti-mouse IGG, peroxidase conjug., Sigma, St. Louis, MO, USA	1/3,000